FORSCHUNGSZENTRUM
ROSSENDORF e.V.

FZR

FZR-139
May 1996
Preprint

E. Persson, T. Gorin and I. Rotter

Decay rates of resonance states at high level density

Forschungszentrum Rossendorf e.V.
Postfach 51 01 19 · D-01314 Dresden
Bundesrepublik Deutschland

Telefon (0351) 260 3281
Telefax (0351) 260 3700
E-Mail rotter@fz-rossendorf.de

Decay rates of resonance states at high level density

E. Persson, T. Gorin and I. Rotter

Forschungszentrum Rossendorf, Institut für Kern-und Hadronenphysik, D-01314 Dresden, Germany
and
Technische Universität Dresden, Institut für Theoretische Physik, D-01062 Dresden, Germany

Abstract

The time dependent Schrödinger equation of an open quantum mechanical system is solved by using the stationary bi-orthogonal eigenfunctions of the non-Hermitean time independent Hamilton operator. We calculate the decay rates at low and high level density in two different formalism. The rates are, generally, time dependent and oscillate around an average value due to the non-orthogonality of the wavefunctions. The decay law is studied disregarding the oscillations. In the one-channel case, it is proportional to t^{-b} with $b \approx 3/2$ in all cases considered, including the critical region of overlapping where the non-orthogonality of the wavefunctions is large. Starting from the shell model, we get $b \approx 2$ for 2 and 4 open decay channels and all coupling strengths to the continuum. When the closed system is described by a random matrix, $b \approx 1 + K/2$ for $K = 2$ and 4 channels. This law holds in a limited time interval. The distribution of the widths is different in the two models when more than one channel are open. This leads to the different exponents b in the power law. Our calculations are performed with 190 and 130 states, respectively, most of them in the critical region. The theoretical results should be proven experimentally by measuring the time behaviour of de-excitation of a realistic quantum system.

1 Introduction

The decay properties of quantum systems at high level density are discussed in the literature with a renewed interest. Such systems are *open* systems. The environment is the energy continuum of decay channels into which the discrete states of the closed system are embedded and which gives them a finite lifetime.

In [1, 2, 3] the decay law is studied analytically for an infinite number of states. It is exponential in the many-channel case but proportional to $t^{-3/2}$ in the one-channel case. More generally, it holds $t^{-1-K/2}$ for a finite number K of channels. The decay rates of a quantum system at low and high level density are studied in [4]. They are shown to saturate at high level density. This result has been interpreted by the authors as a breakdown of the optical model at high level density. In [5] is, however, shown that the saturation corresponds to the trapping effect observed in many different physical systems at high level density, and that the optical model does not break down. The trapping effect studied in many papers (e.g. [6]) creates a separation of the time scales at a critical value of the degree of resonance overlapping. In another investigation [7], the survival and decay probabilities of high Rydberg states are studied. The decay law of states at high level density in nuclei is studied in [8].

All these investigations of the time behaviour of a decaying system are performed on the basis of the random-matrix theory. Thus the question remains open whether similar results will be obtained if the calculations are performed in the framework of a more realistic formalism. Further, some of the results mentioned above show a smooth time dependence of the decay probability while others have an oscillatory behaviour.

In the following, we investigate the decay properties of an open quantum system in detail in order to see not only the monotonic evolution but also the oscillations. We use the continuum shell model (CSM) as well as the statistical model (STM) and compare the results obtained. In Sect. 2, the formalism for deriving the decay rates at high level density is sketched. The properties of the non-Hermitean Hamilton operator are described in detail. At high level density, the decay rates are time dependent functions. In Sect. 3 the quantal coherence creating a redistribution in the system under critical conditions (trapping effect) is described. Here the wavefunctions of the single resonances are no longer orthogonal to each other due to the non-Hermiticity of the Hamilton operator. Numerical results for the decay rates at low and high level density are given in Sect. 4. By means of a simple case (two resonances and one open decay channel), the time dependence of the decay rates as well as the relation between the decay rates and the widths of the resonance states at high level density is illustrated. Further, calculations are performed for many resonances and a few channels. The decay rates oscillate around an average value due to the non-orthogonality of the wavefunctions. In Sect. 5, the decay law ist studied numerically. In the one-channel case, we see a power law in both the CSM and STM for all values of the coupling strength including the critical region. In the last section, some general conclusions on the decay properties of open quantum systems are drawn.

2 Model

2.1 Stationary solution of the Schrödinger equation

The Hamiltonian of an open quantum system is

$$\mathcal{H} = H_{QQ} + V_{QP}\, G_P^{(+)}\, V_{PQ}\ , \tag{1}$$

where

$$H_{QQ} = H^0_{QQ} + V_{QQ} \tag{2}$$

is the Hamiltonian of the closed system,

$$(H_{QQ} - E_R^{SM})\, \Phi_R^{SM} = 0\ , \tag{3}$$

V is the residual interaction between two (bound or unbound) particles of the system, $G_P^{(+)}$ is the Green function for the motion of the particle in the energy continuum of decay channels and $V_{QP} = H_{QP}$, $V_{PQ} = H_{PQ}$ due to the orthogonality of the wavefunctions of the discrete and continuous states. The operators Q and P project onto the subspaces of the discrete and continuous states, respectively,

$$Q = \sum_{R=1}^{N} |\Phi_R^{SM}\rangle\, \langle \Phi_R^{SM}| \tag{4}$$

and

$$P = \sum_{c=1}^{\Lambda} \int_{\epsilon_c}^{\infty} dE\, |\xi_E^{c(+)}\rangle\, \langle \xi_E^{c(+)}|\ . \tag{5}$$

Here, the ξ_E^c are coupled channel wavefunctions in which the channel-channel coupling V_{PP} is involved

$$(H_{PP} - E)\, \xi_E^c = 0\ , \tag{6}$$

$H_{PP} = H^0_{PP} + V_{PP}$. Further, N is the number of discrete states and Λ the number of open and closed decay channels.

In our investigations, $P+Q = 1$. The division into the two subspaces is made by including all resonance phenomena into the Q subspace with the consequence that the wavefunctions of the P subspace depend smoothly on energy in the region considered. Therefore, spectroscopic investigations make sense, i.e. the eigenvalues of $\mathcal{H}$ have a physical meaning [9]. Diagonalizing $\mathcal{H}$, eq. (1),

$$\mathcal{H}\, \tilde{\Phi}_R = (\tilde{E}_R - \frac{i}{2}\tilde{\Gamma}_R)\, \tilde{\Phi}_R\ , \tag{7}$$

we get the energy dependent eigenfunctions $\tilde{\Phi}_R$ and eigenvalues $\tilde{E}_R - \frac{i}{2}\,\tilde{\Gamma}_R$ from which the positions E_R and widths Γ_R of the resonance states R can be determined by solving the fixpoint equations [9]. The energy dependence of the $\tilde{E}_R$ and $\tilde{\Gamma}_R$ is smooth up to threshold effects in the $\tilde{\Gamma}_R$ [11, 12]. Therefore, far from thresholds $E_R \approx \tilde{E}_R(E_0)$ and $\Gamma_R \approx \tilde{\Gamma}_R(E_0)$ where E_0 is a certain energy in the middle of the region considered.

The right and left eigenfunctions of a non-Hermitean Hamilton operator are different from each other. Suppose

$$\mathcal{H}|\tilde{\Phi}_R^{right}\rangle = \tilde{\mathcal{E}}_R\,|\tilde{\Phi}_R^{right}\rangle\,. \tag{8}$$

Then, by multiplying (8) to the left with $\langle\tilde{\Phi}_{R'}^{left}|$ we get

$$\begin{aligned}\langle\tilde{\Phi}_{R'}^{left}|\mathcal{H}|\tilde{\Phi}_R^{right}\rangle &= \tilde{\mathcal{E}}_R\,\langle\tilde{\Phi}_{R'}^{left}|\tilde{\Phi}_R^{right}\rangle\cdot \\ &= \tilde{\mathcal{E}}_R\,\delta_{RR'}\,,\end{aligned} \tag{9}$$

where the orthogonality of $\langle\tilde{\Phi}_{R'}^{left}|$ and $|\tilde{\Phi}_R^{right}\rangle$ is assumed. From (9) it follows

$$\langle\tilde{\Phi}_R^{left}|\mathcal{H} = \tilde{\mathcal{E}}_R\,\langle\tilde{\Phi}_R^{left}|\,, \tag{10}$$

which is the time independent Schrödinger equation for the left state. One gets from eq. (10)

$$\mathcal{H}^\dagger(\langle\tilde{\Phi}_R^{left}|)^\dagger = \tilde{\mathcal{E}}_R^*\,(\langle\tilde{\Phi}_R^{left}|)^\dagger\,. \tag{11}$$

In the case of a Hermitean Hamiltonian, $H^\dagger = H$, it imediately follows from (11) by comparison with (8) that $\tilde{\mathcal{E}}_R$ is real and $\tilde{\Phi}_R^{left} = \tilde{\Phi}_R^{right}$. In our case, eq. (1), the Hamiltonian is non-Hermitean, $H^\dagger \neq H$. The non-diagonal matrix elements $\sum_c \int dE\ \langle\Phi_R^{SM}|V|\xi_E^c\rangle\cdot G_P^{(+)}\cdot\langle\xi_E^c|V|\Phi_{R'}^{SM}\rangle$ of $\mathcal{H}$ are, however, symmetric in relation to R and R' since the Φ_R^{SM} are real. Therefore, $\mathcal{H}^\dagger = \mathcal{H}^*$. By taking the complex conjugate of (11) and comparing with (8), we get $\tilde{\Phi}_R^{left*} = \tilde{\Phi}_R^{right}$.

Therefore, the left eigenfunctions of $\mathcal{H}$ are $\langle\tilde{\Phi}_R^*|$ if the right ones are denoted by $|\tilde{\Phi}_R\rangle$. As a consequence, we have

$$\langle\tilde{\Phi}_{R'}^{left}|\tilde{\Phi}_R^{right}\rangle = \langle\tilde{\Phi}_{R'}^*|\tilde{\Phi}_R\rangle = \delta_{RR'} \tag{12}$$

where both $\tilde{\Phi}_{R'}^*$ and $\tilde{\Phi}_R$ are taken at the same energy E. Further, it follows from (12) that

$$\langle\tilde{\Phi}_R|\tilde{\Phi}_R\rangle \geq 1\,, \tag{13}$$

and that $\langle\tilde{\Phi}_{R'}|\tilde{\Phi}_R\rangle$ is generally nonzero and complex for $R \neq R'$.

For spectroscopic investigations to make sense, we need that $\langle\tilde{\Phi}_{R'}^*(E_{R'})|\tilde{\Phi}_R(E_R)\rangle \approx \delta_{RR'}$. This condition is fulfilled only if the $\tilde{\Phi}_R$ are nearly energy independent. In such a case, the relation (12) holds to a good approximation also if every $\tilde{\Phi}_R$ is taken at the energy E_R of the resonance state R [9].

In the CSM, both the real and imaginary parts of $V_{QP}G_P^{(+)}V_{PQ}$ in (1) are taken into account,

$$\mathcal{H} = H_{QQ} + \Re\{V_{QP}G_P^{(+)}V_{PQ}\} + i\,\Im\{V_{QP}G_P^{(+)}V_{PQ}\} \tag{14}$$

where H_{QQ} given by eq. (2) is a standard nuclear shell model Hamiltonian with spin-orbit coupling and zero-range forces [9, 11], $G_P^{(+)} = P(E-(H_{PP}^0+V_{PP}))^{-1}P$ is the Green function in the P subspace, and the energy dependent matrix elements $\langle\Phi_R^{SM}|V|\xi_E^c\rangle$ are calculated for all resonance states R and decay channels c. They contain the parameter α which is varied in order to investigate the behaviour of the system as a function of the coupling strength between the discrete states and the continuum [11]. It is

$V_{QP} = \alpha V^0_{QP}$, $V_{PQ} = \alpha V^0_{PQ}$, $V_{PP} = \alpha V^0_{PP}$, but $V_{QQ} = V^0_{QQ}$. A variation of the parameter α leads also to energy shifts which are large especially for the broad resonances.

These energy shifts do not appear in the STM [13]. This model is used generally for the description of a group of states lying all in a relatively narrow energy region far from thresholds. Thus, it is justified to choose the coupling matrix elements $\langle \Phi^{SM}_R | V | \xi^c_E \rangle$ energy independent. Further, we neglect the channel-channel coupling. It is also assumed that $\Re\{V_{QP} G^{(+)}_P V_{PQ}\}$ is energy independent and is effectively taken into account together with V_{QQ} in diagonalizing the Hamiltonian H'_{QQ} of the corresponding closed system, i.e.

$$H'_{QQ} = H^0_{QQ} + V_{QQ} + \Re\{V_{QP} G^{(+)}_P V_{PQ}\} \,. \tag{15}$$

H'_{QQ} is drawn from the Gaussian orthogonal ensemble (GOE). Then, the relation between the Hamilton operator $\mathcal{H}'$ of the open system and H'_{QQ} of the closed system reduces to

$$\begin{aligned} \mathcal{H}' &= H'_{QQ} + i\, \Im\{V_{QP} G^{(+)}_P V_{PQ}\} \\ &= H'_{QQ} - i\pi \cdot V\, V^+ \,. \end{aligned} \tag{16}$$

The average coupling matrix element $v_c^2 = \frac{1}{N} \sum_{i=1}^{N} |V_i^c|^2$ contains the vectors V^c with components $V_i^c = \langle \Phi_i | \sqrt{\alpha} \hat{V} | \chi_c \rangle$ [14]. In our calculations, either the elements V_i^c are randomly chosen or the vectors V^c are constructed orthogonal with random length. In the first case, the orthogonality is fulfilled with sufficient accuracy for $N \gg K$ where K is the number of open decay channels. The coupling matrix element v_c^2 is a measure of the average coupling strength of a discrete state Φ_i (eigenfunction of H'_{QQ}) to the channel χ_c. It can be varied by means of the coupling parameter α.

2.2 Time dependent equations

Considering the case of overlapping resonances, we represent the time dependent wavefunction of an ensemble of states by

$$|\phi(t)\rangle = \sum_R a_R(t)\, |\tilde{\Phi}_R\rangle \tag{17}$$

where the $\tilde{\Phi}_R$ are eigenfunctions of $\mathcal{H}$, eq. (1). Then the time dependent Schrödinger equation reads

$$i\hbar \frac{d}{dt} |\phi(t)\rangle = \mathcal{H}\, |\phi(t)\rangle \tag{18}$$

and

$$\begin{aligned} |\phi(t)\rangle &= e^{-\frac{i}{\hbar}\mathcal{H}\, t}\, |\phi(0)\rangle \\ &= \sum_R a_R(0) e^{-\frac{i}{\hbar}(\tilde{E}_R - \frac{i}{2}\tilde{\Gamma}_R)\, t}\, |\tilde{\Phi}_R\rangle \,. \end{aligned} \tag{19}$$

The equation for $\langle \phi(t)|$ is

$$\begin{aligned} \langle \phi(t)| &= \langle \phi(0)|\, e^{\frac{i}{\hbar}\mathcal{H}^\dagger\, t} \\ &= \sum_R a_R(0)^* e^{\frac{i}{\hbar}(\tilde{E}_R + \frac{i}{2}\tilde{\Gamma}_R)\, t}\, \langle \tilde{\Phi}_R| \,. \end{aligned} \tag{20}$$

The justification of (17) and (18) consists in the following:
(i) It is assumed that $\tilde{E}_R$, $\tilde{\Gamma}_R$ and $\tilde{\Phi}_R$ are almost independent of energy in the region considered.
(ii) As shown in [9], the wavefunction of a resonance state is

$$\begin{aligned}\tilde{\Omega}_R &= \tilde{\Phi}_R + \sum_c \int_{\epsilon_c}^{\infty} dE' \xi^c_{E'} \, (E^{(+)} - E')^{-1} \, \langle \xi^c_{E'} | V | \tilde{\Phi}_R \rangle \\ &= (1 + G_P^{(+)} V) \, \tilde{\Phi}_R \end{aligned} \tag{21}$$

but not $\tilde{\Phi}_R$. The wavefunctions χ^c_E of the channels c and the coupled channel wavefunctions ξ^c_E, defined by eq. (6), are related by

$$\xi^c_E = (1 + G_P^{(+)} \, V) \, \chi^c_E \, . \tag{22}$$

It follows therefore for the coupling matrix element of the resonance state R (with the wavefunction $\tilde{\Omega}_R$) to the channel c (with the wavefunction χ^c_E) the relation [10]

$$\langle \tilde{\Omega}_R | V | \chi^c_E \rangle = \langle \tilde{\Phi}_R | V | \xi^c_E \rangle \, . \tag{23}$$

In our formulation (with the Hamiltonian $\mathcal{H}$ of the CSM), the channel coupling is contained in the basic wavefunctions ξ^c_E of the P subspace, eq. (5), in the same manner as configurational mixing is involved in the basic wavefunctions Φ^{SM}_R of the Q subspace, eq. (4). In the representation (17), the eigenfunctions $\tilde{\Phi}_R$ of $\mathcal{H}$ should be used, therefore, and *not* the wavefunctions $\tilde{\Omega}_R$ of the resonance states.

Using (19) and (20), the population probability is as follows. Since $\langle \tilde{\Phi}_{R'} | \tilde{\Phi}_R \rangle \neq \delta_{RR'}$, generally, we have

$$\langle \phi(t) | \phi(t) \rangle = \sum_{RR'} a_R(0) a_{R'}(0)^* \, e^{-\frac{i}{\hbar}(E_R - E_{R'} - \frac{i}{2}(\Gamma_R + \Gamma_{R'}))\, t} \, \langle \tilde{\Phi}_{R'} | \tilde{\Phi}_R \rangle \tag{24}$$

which can be rewritten as

$$\begin{aligned}\langle \phi(t) | \phi(t) \rangle &= \sum_R |a_R(0)|^2 \, e^{-\frac{1}{\hbar}\Gamma_R \, t} \, \langle \tilde{\Phi}_R | \tilde{\Phi}_R \rangle \\ &\quad + 2 \sum_{R<R'} e^{-\frac{1}{2\hbar}(\Gamma_R + \Gamma_{R'})\, t} \times \\ &\quad \Re \Big\{ a_R(0) a_{R'}(0)^* e^{-\frac{i}{\hbar}(E_R - E_{R'})\, t} \langle \tilde{\Phi}_{R'} | \tilde{\Phi}_R \rangle \Big\} \, . \end{aligned} \tag{25}$$

A decay rate k^{eff} can be defined by

$$k^{eff}(t) = -\frac{d}{dt} \, ln \langle \phi(t) | \phi(t) \rangle \tag{26}$$

which is in general a complicated time dependent function. It has a monotonic behaviour according to the first sum (single sum over R) in (25) and a oscillating one arising from the second sum (double sum over R, R').

To study the gross time behaviour of k^{eff} we define k^{eff}_{gr} taking into account only the single sum over R,

$$\begin{aligned} k^{eff}_{gr}(t) &= -\frac{d}{dt} \, ln \Big\{ \sum_R |a_R(0)|^2 \, e^{-\Gamma_R \, t/\hbar} \langle \tilde{\Phi}_R | \tilde{\Phi}_R \rangle \Big\} \\ &= \frac{1}{\hbar} \, \frac{\sum_R |a_R(0)|^2 \, \Gamma_R \, e^{-\Gamma_R \, t/\hbar} \langle \tilde{\Phi}_R | \tilde{\Phi}_R \rangle}{\sum_R |a_R(0)|^2 \, e^{-\Gamma_R \, t/\hbar} \langle \tilde{\Phi}_R | \tilde{\Phi}_R \rangle} \, . \end{aligned} \tag{27}$$

Only under the condition $\langle\tilde{\Phi}_{R'}|\tilde{\Phi}_R\rangle \approx 0$ for $R' \neq R$ (see Fig. 1 in Sect. 3) we get $k^{eff} \approx k_{gr}^{eff}$.

In the case of an isolated resonance R, (26) reduces to the standard relation $k^{eff} = k_R^{eff} = \frac{1}{\hbar}\Gamma_R$ between decay rate and width. In this case, k^{eff} is time independent and the decay law is exponential.

The shape of isolated resonances is of Breit-Wigner type. Therefore, we calculate the coefficients $|a_R(0)|^2$ in (25) and (27) from the overlap integrals between Breit-Wigner distributed resonances R and an incoming wave, chosen Gaussian distributed with energy E_b and width Γ_b:

$$|a_R(0)|^2 = F^{-1} \int dE \, \frac{\frac{1}{4}\Gamma_R^2}{(E-E_R)^2 + \frac{1}{4}\Gamma_R^2} \cdot e^{-\left((E-E_b)/\Gamma_b\right)^2} \tag{28}$$

where the normalization factor is $F = \int dE \, e^{-((E-E_b)/\Gamma_b)^2} = \sqrt{\pi} \cdot \Gamma_b$. The $a_R(0)$ used in the double sum in (27) are calculated as the positive root of $\sqrt{|a_R(0)|^2}$ i.e. any initial phase from the excitation is ignored. A very small Γ_b simplifies the expression (28):

$$|a_R(0)|^2 \approx \frac{\frac{1}{4}\Gamma_R^2}{(E_b-E_R)^2 + \frac{1}{4}\Gamma_R^2} \, . \tag{29}$$

For a very large Γ_b, $|a_R(0)|^2 \approx \Gamma_R$.

It should be noted here that the nucleus is not necessarily excited via one of the channels c which define the P subspace of decay channels. It may be excited via another mechanism such as, e.g., the deexcitation of a heavier nucleus.

3 Quantal coherence

3.1 Trapping of resonance states at high level density

The trapping effect observed in many investigations (for references see [6]), appears if the second part of the Hamiltonian (1) becomes important relative to the first one. This implies that the non-diagonal matrix elements are large with the result that the diagonal matrix elements differ essentially from the eigenvalues. Since the trace is constant at a fixed energy E of the system and coupling strength α between discrete states and continuum, we have

$$-2\,\Im\{tr(\mathcal{H}(E,\alpha))\} = \sum_{R=1}^{N}\sum_{c=1}^{K}\gamma_{Rc}(E,\alpha) = \sum_{R=1}^{N}\tilde{\Gamma}_R(E,\alpha) \equiv \gamma(E,\alpha) \tag{30}$$

where c denote the K open decay channels and

$$\gamma_{Rc}^{1/2} = (2\pi)^{1/2}\,\langle\Phi_R^{SM}|V|\xi_E^c\rangle \tag{31}$$

is the coupling matrix element between the discrete state R and the channel c. It should be mentioned here that $\gamma_{Rc}^{1/2}$ may be very different from the amplitude of the partial width

$$\tilde{\Gamma}_{Rc}^{1/2} = (2\pi)^{1/2}\,\frac{\langle\tilde{\Phi}_R|V|\xi_E^c\rangle}{\langle\tilde{\Phi}_R|\tilde{\Phi}_R\rangle} \tag{32}$$

of the resonance state R, even if $\langle\tilde{\Phi}_R|\tilde{\Phi}_R\rangle = 1$ [9, 11].

With increasing coupling strength α the widths Γ_R of all states increase until the diagonal matrix elements of the Hamiltonian (1) and its eigenvalues start to differ essentially from one another. Here, the imaginary parts $\tilde{\Gamma}_R$ of K eigenvalues start to increase much stronger than the coupling matrix elements γ_{Rc}. This is possible only at the cost of the $\tilde{\Gamma}_R$ of the $N-K$ remaining states (*trapping effect*) which can be seen from eq. (30) rewritten in the following manner

$$\frac{\sum_{R=1}^{K}\tilde{\Gamma}_R(E,\alpha)}{\gamma(E,\alpha)} = 1 - \frac{\sum_{R=K+1}^{N}\tilde{\Gamma}_R(E,\alpha)}{\gamma(E,\alpha)} \,. \tag{33}$$

Eq. (33) holds for all α. We define the critical region as that region where the reorganization takes place and characterize it by a value α_{crit} in its middle.

Due to the trapping effect, different time scales are formed above the critical region (at high level density)

$$\sum_{R=1}^{K}\tilde{\Gamma}_R \;\gg \sum_{R=K+1}^{N}\tilde{\Gamma}_R \,. \tag{34}$$

It also holds

$$\frac{1}{K}\sum_{R=1}^{K}\tilde{\Gamma}_R \;\gg \frac{1}{N-K}\sum_{R=K+1}^{N}\tilde{\Gamma}_R \,. \tag{35}$$

The relations (34) and (35) are a consequence of the fact that the rank of H_{QQ} in (1) is N while that of the imaginary part of the second term $V_{QP}G_P^{(+)}V_{PQ}$ is $K < N$ (if separability holds). Thus, a redistribution must take place in the transition from low level density where the first term of the Hamiltonian (1) is important, to high level density where the second part becomes important.

In the random matrix model (STM) with the Hamiltonian $\mathcal{H}'$, a critical point can be defined by $\kappa \equiv 2\bar{\Gamma}/(KD) = 1$ (for $K \ll N$) where $\bar{\Gamma}$ is the average value of the widths of the N resonance states and D is their average distance [15, 17]. At this critical point, $\sum_{R=K+1}^{N}\Gamma_R$ starts to decrease with increasing α [16].

In the CSM (continuum shell model), a critical point cannot be defined by $\kappa = 1$. The trapping of resonances occurs locally between individual resonances for which a critical point in the complex plane is well defined. But fluctuations in the level density can, as a rule, not be described by a simple law. This leads to uncertainties in the definition of a global critical point [6]. Thus we restrict ourselves, in the framework of this model, to the definition of a critical region (instead of a critical point) in which the separation of the time scales takes place.

In the CSM with the Hamiltonian $\mathcal{H}$ the separation of the time scales takes place at $\kappa \approx 1$ only in the one-channel case. In the many-channel case, the time scales are well separated already at $\kappa < 1$ [18]. A reason for this behaviour is surely the term $\Re\{V_{QP}G_P^{(+)}V_{PQ}\}$ which appears explicitely in $\mathcal{H}$ of the CSM, eq. (14). The symmetry properties of this term are determined by the channels and their coupling to one another. Its matrix elements are not small. The critical region in which the second term of $\mathcal{H}$ becomes the dominant part is

reached therefore at coupling parameters α (and the corresponding overlapping parameters κ) which are smaller than in the case of $\mathcal{H}'$ without such a term. The differences between the values of α_{crit} (or κ_{crit}) belonging to the two Hamiltonians are larger for a larger number of (coupled) decay channels: κ_{crit} decreases with K in the CSM. In the STM, however, $\kappa_{crit} = 1$ for $K \ll N$ while for K not small in comparison with N, we even have $\kappa_{crit} > 1$.

The term $\Re\{V_{QP} G_P^{(+)} V_{PQ}\}$ creates, moreover, energy shifts of all the states. Therefore, $\sum_{R=K+1}^{N} \tilde{\Gamma}_R$ does not decrease [11] as in the STM. The energy shifts due to $\Re\{V_{QP} G_P^{(+)} V_{PQ}\}$ may also lead to level repulsions in the complex plane between trapped states. Thus, a second generation of short-lived states [11] can be created.

3.2 Wavefunctions in the critical region

The redistribution in the system (*trapping effect*) takes place in a critical region of the level density (in relation to the average width of the states) [9, 11] in which the wavefunctions of the short-lived states align with the channel wavefunctions [6]. In this critical region, the left and right eigenfunctions of $\mathcal{H}$ differ substantially from each other. Thus, the redistribution taking place in the system reflects itself in the non-orthogonality of the $\tilde{\Phi}_R$ [11].

Beyond the critical region, the wavefunctions of the K short-lived states point into the direction of the decay channels [6]. They are orthogonal to one another as the channel wavefunctions and are orthogonal also to the wavefunctions of the trapped states. The wavefunctions of the $N - K$ trapped long-lived states calculated with the full Hamiltonian $\mathcal{H}$ (14), retain partly the non-orthogonality. These investigations have been performed for the diagonal matrix elements $\langle \tilde{\Phi}_R | \tilde{\Phi}_R \rangle$ [11].

The behaviour of $|\langle \tilde{\Phi}_{R'} | \tilde{\Phi}_R \rangle|$ is illustrated in Fig. 1. The calculations are performed in the framework of the CSM (Fig. 1.a to 1.c) as well as in the STM (Fig. 1.d). In all calculations we have $N = 70$ states and $K = 1$ open decay channel. The figure shows $|\langle \tilde{\Phi}_{R'} | \tilde{\Phi}_R \rangle| - \delta_{RR'}$, i.e. the *deviations* of $\langle \tilde{\Phi}_{R'} | \tilde{\Phi}_R \rangle$ from $\langle \tilde{\Phi}^*_{R'} | \tilde{\Phi}_R \rangle = \delta_{RR'}$, for all combinations R, R' of the 70 states.

In Fig. 1.a, it is $\alpha < \alpha_{crit}$, whereas in Figs. 1.b and 1.c $\alpha = \alpha_{crit}$ and $\alpha > \alpha_{crit}$, respectively. Well below α_{crit} the deviations of $\langle \tilde{\Phi}_{R'} | \tilde{\Phi}_R \rangle$ from $\delta_{RR'}$ are small, but in and *above* the critical region, the deviations are large.

Fig. 1.d is made in the STM at the critical point $\kappa = 1$. The figure shows large deviations from $\delta_{RR'}$. Other calculations have shown that below *as well as* above the critical point, the deviations are small in this model.

The plots of Fig. 1 show, that in the critical region the value $|\langle \tilde{\Phi}_{R'} | \tilde{\Phi}_R \rangle| - \delta_{RR'}$ is always large. Well below the critical region $|\langle \tilde{\Phi}_{R'} | \tilde{\Phi}_R \rangle| \approx \delta_{RR'}$ in all cases considered. In the STM, $|\langle \tilde{\Phi}_{R'} | \tilde{\Phi}_R \rangle|$ is small also far beyond the critical region. In the CSM, however, this value remains large for the trapped states. This difference is caused by the term $\Re\{V_{QP} G_P^{(+)} V_{PQ}\}$ in $\mathcal{H}$, eq. (14) (see Section 3.1).

4 Decay rates at low and high level density

4.1 Two resonances and one open decay channel

In order to investigate the relation (25) in detail at high level density, we performed some calculations.

First, we consider the case with two resonances and one open decay channel. This simple example allows to illustrate the time dependence of k^{eff}.

The Hamiltonian is taken according to (16) . It reads [6]

$$\mathcal{H}' = \begin{pmatrix} 1 & 0 \\ 0 & -1 \end{pmatrix} - 2i\alpha \begin{pmatrix} \cos^2\varphi & \cos\varphi\sin\varphi \\ \cos\varphi\sin\varphi & \sin^2\varphi \end{pmatrix}. \tag{36}$$

Without loss of generality we have chosen the eigenvalues of H_{QQ} to be ± 1. The V in (16) are chosen as $V = \sqrt{\frac{2\alpha}{\pi}}(\cos\varphi, \sin\varphi)$ with $\varphi = \pi/8$. Thus, the coupling of one of the resonance states to the decay channel is stronger than that of the other one.

The influence of the parameter α in the Hamiltonian (36) onto the eigenvalue picture is illustrated by means of Fig. 2.a. The "motion" of the eigenvalues is drawn here as a function of the coupling strength α. One observes the trapping effect, i.e. an attraction of the real parts of the eigenvalues and a repulsion in the imaginary parts for $\alpha \approx \alpha_{crit}$.

In the case of two resonances, $\langle\phi(t)|\phi(t)\rangle$, eq. (25), consists of three terms,

$$\begin{aligned} \langle\phi(t)|\phi(t)\rangle \;=\; & |a_{br}(0)|^2\, e^{-\frac{1}{\hbar}\Gamma_{br}\,t}\,\langle\tilde{\Phi}_{br}|\tilde{\Phi}_{br}\rangle \;+ |a_{tr}(0)|^2\, e^{-\frac{1}{\hbar}\Gamma_{tr}\,t}\,\langle\tilde{\Phi}_{tr}|\tilde{\Phi}_{tr}\rangle \\ & + 2e^{-\frac{1}{2\hbar}(\Gamma_{br}+\Gamma_{tr})t}\,\Re\{a_{br}(0)a_{tr}(0)^* e^{-\frac{i}{\hbar}(E_{br}-E_{tr})t}\langle\tilde{\Phi}_{br}|\tilde{\Phi}_{tr}\rangle\}\,. \end{aligned} \tag{37}$$

Here, the index br stands for the broader of the two states and the index tr for the narrower one.

In Fig. 2.b, $|a_R(0)|^2$, eq. (28), is shown as a function of α for two cases: (i) the beam energy is equal to the energy of the narrow state, $E_b = E_{tr}$, and (ii) it is equal to the energy of the broad state, $E_b = E_{br}$. In both cases the beam is delta-shaped, and the maximum value $|a_1(0)|^2 = 1$ (marked with a star) is obtained for the chosen state in both cases. The up triangles stand for the broad state of case (i) and the down triangles for the narrow state of case (ii). For small α, almost only the chosen state is excited. As $\alpha \to \alpha_{crit}$, $|a_2(0)|^2$ for the other state grows in both cases. As α grows further beyond α_{crit}, $|a_2(0)|^2 \to 1$ in (i), but $|a_2(0)|^2 \to 0$ in (ii). This is a direct reflection of the trapping effect.

In Fig. 2, the three points marked correspond to $\alpha \ll \alpha_{crit}$, $\alpha \approx \alpha_{crit}$ and $\alpha > \alpha_{crit}$. For these three values of α, k^{eff} and k_{gr}^{eff} are calculated. It is $\bar{\Gamma}/D = 0.1$, 1.1 and 4.1 respectively, in these three cases. The results are shown in Fig. 3 for $E_b = E_{tr}$ and in Fig. 4 for $E_b = E_{br}$. It is $\alpha \ll \alpha_{crit}$ in Figs. 3.a and 4.a, $\alpha \approx \alpha_{crit}$ in Figs. 3.b and 4.b and $\alpha > \alpha_{crit}$ in Figs. 3.c and 4.c. The thick lines represent k_{gr}^{eff} and the thin ones k^{eff}. In all cases, k^{eff} oscillates around k_{gr}^{eff} or it is $k^{eff} \approx k_{gr}^{eff}$. Note the different ordinate and abscissa scales in the different plots.

In Fig. 3.a, k_{gr}^{eff} is constant: $k_{gr}^{eff} = \Gamma_{tr}$. This arises from the small value of the first term in (37) caused by the small value $|a_{br}(0)|^2$. k^{eff} however shows a periodical behaviour

caused by the interference term. It follows from (37) that the period is $T = 2\pi\hbar/\Delta E$ where $\Delta E = |E_{tr} - E_{br}|$. In our case, $\Delta E = 2MeV$, giving $T = 1\pi\hbar/MeV$. This period can be seen in Fig. 3.a. The amplitude of the oscillations decreases in the region showed because the interference term decreases as $exp(-\frac{1}{2}(\Gamma_{br} + \Gamma_{tr})\ t/\hbar)$ while the second term in (37) decreases as $exp(-\Gamma_{tr}\ t/\hbar)$.

At $\alpha \approx \alpha_{crit}$ (Fig. 3.b), k_{gr}^{eff} decreases from a value of about Γ_{br} to Γ_{tr} in a time of about $1\hbar/MeV$. During this time, the broad state almost disappears and $k_{gr}^{eff} = \Gamma_{tr}$ for larger times. There are no long-time oscillations, because the interference term disappears as $exp\{-\frac{\Gamma_{br}}{2\hbar}\ t\}$.

Both k_{gr}^{eff} and k^{eff} decrease faster from the large value at $t = 0$ to Γ_{tr} if α is larger (Fig. 3.c). The time when Γ_{tr} is reached is approximately $0.4\hbar/MeV$ in Fig. 3.c compared to approximatively $1\hbar/MeV$ in Fig. 3.b. The difference between k_{gr}^{eff} and k^{eff} in Fig. 3.c is small because of the large difference between Γ_{br} and Γ_{tr}.

In Fig. 4.a, k_{gr}^{eff} is nearly constant for $t < 20\hbar/MeV$ for the same reasons as in fig. 3.a. The value of k_{gr}^{eff} is however $\Gamma_{br}/\hbar$ corresponding to the *broad* state. Since the broad state decays quickly, k_{gr}^{eff} decreases to $\Gamma_{tr}/\hbar$ of the *narrow* state at about $t = 30\hbar/MeV$. The time when the first two terms in (37) are equal is $t = 29.8\hbar/MeV$. The period of the oscillation is $1\pi\hbar/MeV$ also in this case. The amplitude is large around $t = 30\hbar/MeV$ but small for other times. This follows from (37): For small times, the interference term is small due to $a_{br}(0) \gg a_{tr}(0)$ and the decay pattern is determined by only the broad state. At large times, the broad state has almost disappeared and the decay is determined by the narrow state in spite of $a_{br}(0) \gg a_{tr}(0)$. Only in the transition interval, both resonances are of comparable importance and interfere strongly.

In Fig. 4.b, k_{gr}^{eff} starts from an almost constant plateau corresponding to Γ_{br} and decreases to the value of Γ_{tr} during a time $2\hbar/MeV$. Until the time $3\hbar/MeV$, k^{eff} oscillates around k_{gr}^{eff}, but for larger times $k^{eff} \approx k_{gr}^{eff}$.

The plateau at $k_{gr}^{eff} = \Gamma_{br}$ for small times can clearly be seen in Fig. 4.c. In a short time interval, k_{gr}^{eff} decreases to Γ_{tr}. The difference between k^{eff} and k_{gr}^{eff} is small due to the large difference between Γ_{br} and Γ_{tr}.

4.2 N resonances and K channels

In Fig. 5 we show the results of a calculation for $N = 70$ states and $K = 2$ open channels using the STM (Hamiltonian (16)) with randomly chosen coupling vectors V^c. The degree of overlapping of the resonances is large, $\kappa = 10.0$. We have therefore two broad states and 68 trapped ones. The beam is deltashaped and its energy E_b corresponds to the energy E_{tr} of one of the trapped states. The thick line in Fig. 5 shows k_{gr}^{eff} while the thin one is k^{eff}. Also in this case, k^{eff} oscillates around k_{gr}^{eff}.

The difference between the calculation with 70 resonances to that with 2 resonances consists mainly in the fact that $|a_R(0)|^2$ is nonvanishing not only for the two broad states and the trapped one for which $E_b = E_{tr}$ but also for other trapped states in the neighbourhood of E_b. As a consequence, many of the interference terms will be important. This can be seen

in the complicated, overlaid oscillations of k^{eff}. The two broad states vanish very quickly.

Further, some trapped neighbours of the chosen state contribute to eq. (24). Around $t = 50\hbar/MeV$ we can see a transition for k_{gr}^{eff} to a value corresponding to the more longlived states.

In the calculation above, the beam is much narrower than the width of the chosen state which is $\Gamma_b \ll 0.084MeV$. Due to the uncertainity principle, this gives a resolution in time of $\Delta t \approx \frac{\hbar}{\Gamma_b}$. Thus $\Delta t \gg 12\hbar/MeV$.

We performed another calculation with the same 70 states and 2 channels in which the incoming beam is much broader than the energy interval in which the states are lying. This gives $|a_R(0)|^2 \approx \Gamma_R$ for *all* the states. Fig. 6 shows k^{eff} (thin line) and k_{gr}^{eff} (thick line) for this case. In spite of many terms in the double sum of (25), k^{eff} shows a complicated oscillatory behaviour.

The point is that also in this very complicated situation, k^{eff} oscillates around k_{gr}^{eff}. The double sum consists of $N(N-1)/2 = 2415$ terms, each with a phase totally uncorrelated with that of all the other ones. The lengths are also uncorrelated. The double sum however does *not* vanish.

We also studied k^{eff} in the CSM. We considered $K = 1$ open channel and $N = 190$ states with $2p-2h$ nuclear structure and $J^\pi = 1^-$ (for details see [11]) and $\bar{\Gamma}/D = 0.006$. Γ_b is very large. In Fig 7.a, k_{gr}^{eff} (thick line) and k^{eff} (thin line) are shown for the same time interval as that of Figs. 5 and 6. The oscillations are much faster in this plot than those in Fig. 6. This is mainly due to the fact that the spectrum in Fig. 6 covers an interval of $2\hbar/MeV$ but in the calculation presented in Fig. 7 the length of the spectrum is $30MeV$. This implies that the fastes oscillations in this case are 15 times faster than those of Fig. 6.

Fig 7.b presents a calculation for the same setup as in Fig. 7.a but for much larger times. The time unit characteristic of the system is $\tau = \hbar/\bar{\Gamma} = 2.9 \cdot 10^4\hbar/MeV$. k^{eff} is shown in the Figure as a function of τ and the plot is drawn in log-log scale. The calculation of k^{eff} is not made enough dense to catch all oscillations. The scattering of the points around k_{gr}^{eff} gives, however, a measure of how large the osillations are. For very large times k_{gr}^{eff} approaches the width $\Gamma_l/\hbar$ of the narrowest state. We also see in Fig 7.b that k^{eff} fluctuates violently around k_{gr}^{eff} as long as k_{gr}^{eff} is time dependent (not constant).

5 Decay law

Isolated resonances are usually assumed to decay according to an exponential law. It is $k_R^{eff} = \tilde{\Gamma}_R/\hbar$ for the state R where $\tilde{\Gamma}_R$ is time independent (see section 2.2). At high level density, k_R^{eff} has to be replaced by k^{eff}, eq. (26) with (25), which generally is a complicated time dependent function (compare Figs. 3 to 7). Even k_{gr}^{eff}, eq. (27), in which the oscillations are neglected, is time dependent. Deviations from the exponential decay law appear therefore at high level density, as a rule.

In the following, we neglect the oscillations of $\langle\phi(t)|\phi(t)\rangle$, i.e. the double sum in eq. (25).

Suppose we have a power law,

$$\langle\phi(t)|\phi(t)\rangle \propto t^{-b}\,, \tag{38}$$

instead of the exponential one $\langle\phi(t)|\phi(t)\rangle \propto exp\{-\Gamma t/\hbar\}$ in a certain time interval. Then the relation between the decay rate and b is

$$\frac{1}{k_{gr}^{eff}(t)} = \frac{t}{b}\,. \tag{39}$$

According to this equation, the deviations from the exponential decay law can be represented by the rise of $1/k_{gr}^{eff}$ as a function of t from which the exponent b can be determined.

Figs. 4 to 7 show plateaus $k_{gr}^{eff}(t) \approx const$ arising from the different lifetimes of the different states. We expect $k_{gr}^{eff}(t) \propto b/t$ with $b \approx const$ (power decay law) if there are many resonance states due to which the stairs between the different plateaus are smeared out. In the long-time scale however, $k_{gr}^{eff}(t) \approx const$ (exponential decay law) where $const = \Gamma_l/\hbar$ (l stands for the longest-lived state).

In the following, we investigate the decay law numerically in both the CSM and the STM for a finite number N of states and a small number K of open decay channels. In Fig. 8 and 9, we show $1/k_{gr}^{eff}$ as a function of time for different values α of the coupling strength to the continuum and for different K. The time scale is given in units $\tau = \hbar/\bar{\Gamma}$ where $\bar{\Gamma}$ is the average width of all the N resonances.

Fig. 8 shows $1/k_{gr}^{eff}$ calculated in the STM for 130 states (with orthogonal constructed coupling vectors V^c), $\kappa = 1$ (critical point) and $K = 1$ (a), 2 (b), 4 (c) and 9 (d). The beam is very broad. The different curves in each subplot correspond to different random choices of H'_{QQ}.

In all curves a power law is well fullfilled in a certain time interval. In the one-channel case, $b \approx 3/2$. The different curves deviate from each other, especially at times larger than 50τ.

For two channels, the power law with $b \approx 2$ holds quite well until $t \approx 30\tau$, for four channels with $b \approx 2.7$ until $t \approx 8\tau$ and for nine channels with $b \approx 4$ until $t \approx 5\tau$.

In Fig. 8, we have shown the results at the critical value $\kappa = 1$. The results of other calculations well below and well above $\kappa = 1$ are similar to those shown in Fig. 8. In a certain time interval, the power law is well fullfilled. We have $b \simeq 1 + K/2$ for $K = 1$ up to 9.

In [1, 2] the decay law has been studied analytically using the Hamiltonian (16) with an infinite number of states, an infinitely broad beam and κ well below the critical value while in [3] the investigations are performed for all κ. The result is $\langle\phi(t)|\phi(t)\rangle \propto t^{-(1+\frac{K}{2})}$, i.e. $b = \frac{K}{2} + 1$ in the case with K open decay channels. Our numerical results with a finite number of states agree quite well with the formula obtained analytically even in the critical region ($K \leq 4$), where the redistribution of the spectroscopic properties takes place.

In the CSM we have performed calculations for $N = 190$ states and $K = 1$, 2, and 4 channels. The 190 states have $2p - 2h$ nuclear structure and $J^\pi = 1^-$ (for details see [11]). The average distance D between the states is defined by those of the shell model states.

The beam is very broad, i.e. $|a_R(0)|^2 \approx \Gamma_R$.

Fig. 9.a show $1/k_{gr}^{eff}$ for 1 open neutron channel. The different curves correspond to $\bar{\Gamma}/D = 0.00072$, 0.087, 0.32, 0.67, 1.14, 1.71 and 2.38. We see that $b \approx 3/2$ for small times up to about $t = 100\tau$.

In Fig. 9.b, $1/k_{gr}^{eff}$ is drawn for the same 190 states, two open neutron channels and $\bar{\Gamma}/D = 0.0035$, 0.20, 0.70, 1.49, 2.53, 3.80, 5.29 and 6.97. For small times (up to $t \approx 50\tau$) $b \approx 2$. A similar behaviour with $b \approx 2$ is obtained for 4 open channels (two neutron and two proton channels) shown in Fig. 9.c. The 11 curves correspond to $\bar{\Gamma}/D = 0.00392$, 0.00394, 0.00396, 0.0044, 0.0065, 0.016, 0.082, 0.32, 1.20, 4.18 and 57.5. We see a power law with $b \approx 2$ as in the 2-channel case up to $t \approx 50\tau$.

The main difference between the results obtained in the two models consists in the dependence of b on the number K of channels. For $K = 1$ we have $b \approx 3/2$ in both models. For $K = 2$ and 4, $b \approx 2$ in the CSM. In the STM however $b \approx 1 + K/2$ (for $\kappa \neq 1$).

In Fig. 10 the distribution of the widths calculated for $\alpha = 4 > \alpha_{crit}$ and $K = 4$ channels in the CSM is shown (histogram for the $\tilde{\Gamma}_R$). The full line is the best fit to these values by a χ^2 distribution. This fit to the calculated $\tilde{\Gamma}_R$ is quite good. Nevertheless, it corresponds to the one-channel case of the STM. For comparison, we show the χ^2 distribution corresponding to four channels (dashed line).

As can be seen from Fig. 10, the width distribution is very different in the two models. This explains the differences for b obtained in our calculations.

6 Conclusions

In the present paper, we investigated the decay properties of an open many-particle quantum system. The Hamiltonian is non-Hermitean, its eigenfunctions and eigenvalues are complex. The eigenfunctions form a bi-orthogonal system. As a consequence, the wavefunctions of the resonance states are generally non-orthogonal to one another. Near the critical point of rearrangement, some states with short lifetimes align with the decay channels. As a result, their lifetimes become still shorter while the lifetimes of the remaining states become longer. Finally, we have two groups of resonance states with well separated lifetimes.

We calculated the decay rates at low as well as at high level density in the framework of both the continuum shell model and the random-matrix formalism. The rates are proportional to the widths of the resonance states at low level density where they are isolated. At higher level density, the decay rates show an oscillatory behaviour caused by the non-orthogonality of the wavefuntions. Disregarding the oscillations, the rates are, nevertheless, still time dependent functions. This implies deviations from the exponential decay law.

The decay law for an ensemble of states in a certain energy region is non-exponential (proportional to $t^{-3/2}$) for the case of one open channel. This result is obtained in both models and for *all* values of the coupling parameter α between bound and unbound states. It is in agreement with the result of analytical investigations in the random matrix theory

for an infinite number of states [1, 2, 3].

The decay law $t^{-1-K/2}$ holds still good in the two models for $K = 2$ open channels. For more than two channels, the exponent remains nearly constant in the CSM. In the STM, however, the $t^{-1-K/2}$ law holds also quite good for $K = 4$ and even for $K = 9$ far from the critical region.

The distribution of the widths is different in the two models when few channels are open. In the CSM, the distribution for 4 channels cannot be fitted by the appropriate χ^2 distribution for $K = 4$ of the STM. This result explains the differences in the decay law obtained in the two models. The origin of the width distribution in the CSM is a question for further investigations.

Finally, we stress that a direct experimental measurement of the decay properties of quantum systems at high level density is of high interest.

Acknowledgment: Valuable discussions with F.M. Dittes, M. Müller, A. Pelster, G. Soff and V.V. Sokolov are gratefully acknowledged. This work was supported by DAAD and DFG (Ro 922).

References

[1] C. H. Lewenkopf and H. A. Weidenmüller, Ann. Phys. (N. Y.) 212, 53 (1991)

[2] F.M. Dittes, H.L. Harney and A. Müller, Phys. Rev. A 45, 701 (1992)
H. L Harney, F.-M. Dittes and A. Müller, Ann. Phys. (N. Y.) 220, 159 (1992)

[3] F. M. Izrailev, D. Saher and V. V. Sokolov, Phys. Rev. E 49, 130 (1994)
N. Lehmann, D. Saher, V.V. Sokolov and H.J. Sommers, Nucl. Phys. A 582, 223 (1995)

[4] U. Peskin, H. Reisler and W.H. Miller, J. Chem. Phys. 101, 9672 (1994)

[5] I. Rotter, to be published

[6] M. Müller, F.-M. Dittes, W. Iskra and I. Rotter, Phys. Rev. E 52, 5961 (1995)

[7] F. Remacle and R.D. Levine, J. Chem. Phys. 104, 1399 (1996)

[8] S. Drożdż, A. Trellakis and J. Wambach, Phys. Rev. Lett. in press (1996)

[9] I. Rotter, Rep. Prog. Phys. 54, 635 (1991) and references therein

[10] I. Rotter, Ann. Phys. (Leipzig) 38, 221 (1981)

[11] W. Iskra, M. Müller and I. Rotter, J. Phys. G 19, 2045 (1993); G 20, 775 (1994)

[12] E. Persson, M. Müller and I. Rotter, Phys. Rev. C, in press (June 1996)

[13] W. Iskra, I. Rotter and F.-M. Dittes, Phys. Rev. C 47, 1086 (1993)

[14] F.-M. Dittes, I. Rotter and T.H. Seligman, Phys. Lett. A 158, 14 (1991)

[15] F.-M. Dittes, H.L. Harney and I. Rotter, Phys. Lett. A 153, 451 (1991)

[16] T. Gorin, F.M. Dittes, M. Müller and I. Rotter, to be published

[17] V.V. Sokolov and V.G. Zelevinsky, Ann. Phys. (N.Y.) 216, 323 (1992)

[18] I. Rotter, J. Phys. G 14, 857 (1988)

Figure 1

The measure of the non-orthogonality of the states, $|\langle\tilde{\Phi}_{R'}|\tilde{\Phi}_R\rangle| - \delta_{RR'}$, for $N = 70$ states and $K = 1$ open channel. (a), (b) and (c) are calculated in the CSM below ($\alpha = 0.1$), in ($\alpha = 2$) and above ($\alpha = 10$) the critical region of reorganisation, respectively. (d) is in the STM at the critical point.

Figure 2

The complex eigenvalues of $\mathcal{H}'$ for two states and increasing coupling strength α to the continuum (a) and $|a_R(0)|^2$ as a function of α for the two states (b). Up triangles: broad state when narrow state is excited, down triangles: narrow state when broad state excited, stars: the other state in both cases.

Figure 3

The decay rates k^{eff} (thin lines) and k_{gr}^{eff} (thick lines) for $\alpha \ll \alpha_{crit}$ (a), $\alpha \approx \alpha_{crit}$ (b) and $\alpha > \alpha_{crit}$ (c). The curves are for the two states shown in Fig. 2 and $E_b = E_{tr}$.

Figure 4

The same as in Fig. 3 but $E_b = E_{br}$.

Figure 5

The decay rates k_{gr}^{eff} (thick line) and k^{eff} (thin line) in the STM for $N = 70$ states and $K = 2$ open channels, $\kappa = 10$. The beam is narrow and with an energy of one of the trapped states.

Figure 6

The same as in Fig. 5, but the beam is much broader than the spectrum.

Figure 7

The decay rates k_{gr}^{eff} (thick lines) in the CSM with $N = 190$ states ($2p - 2h$ nuclear structure, $J^\pi = 1^-$), $K = 1$ open channel and $\bar{\Gamma}/D = 0.012$. In (a), the oscillations of k^{eff} (thin line) are shown while in (b), only some dots of k^{eff} are given. The time scales are in different units in (a) and (b).

Figure 8

$1/k_{gr}^{eff}$ in the STM for 130 states and $\kappa = 1$. It is $K = 1$ in (a), $K = 2$ in (b), $K = 4$ in (c) and $K = 9$ in (d). The different curves in each plot correspond to different random matrices H'_{QQ}. The units are $\tau = \hbar/\bar{\Gamma}$ (different scaling in all figures).

Figure 9

$1/k_{gr}^{eff}$ in the CSM. The states are the same as in Fig. 7. The different curves in each plot correspond to different $\bar{\Gamma}/D$ (for details, see the text). It is $K = 1$ in (a), $K = 2$ in (b) and $K = 4$ in (c). The units are $\tau = \hbar/\bar{\Gamma}$.

Figure 10

Histogram for the distribution of the widths in the CSM for $K = 4$ and $\alpha = 4$. The full line is the best fit to a χ^2 distribution, which corresponds to one channel in the STM while the dashed line is the STM distribution for 4 channels.

Csm, 190st, 1channel.

Fig. 1a

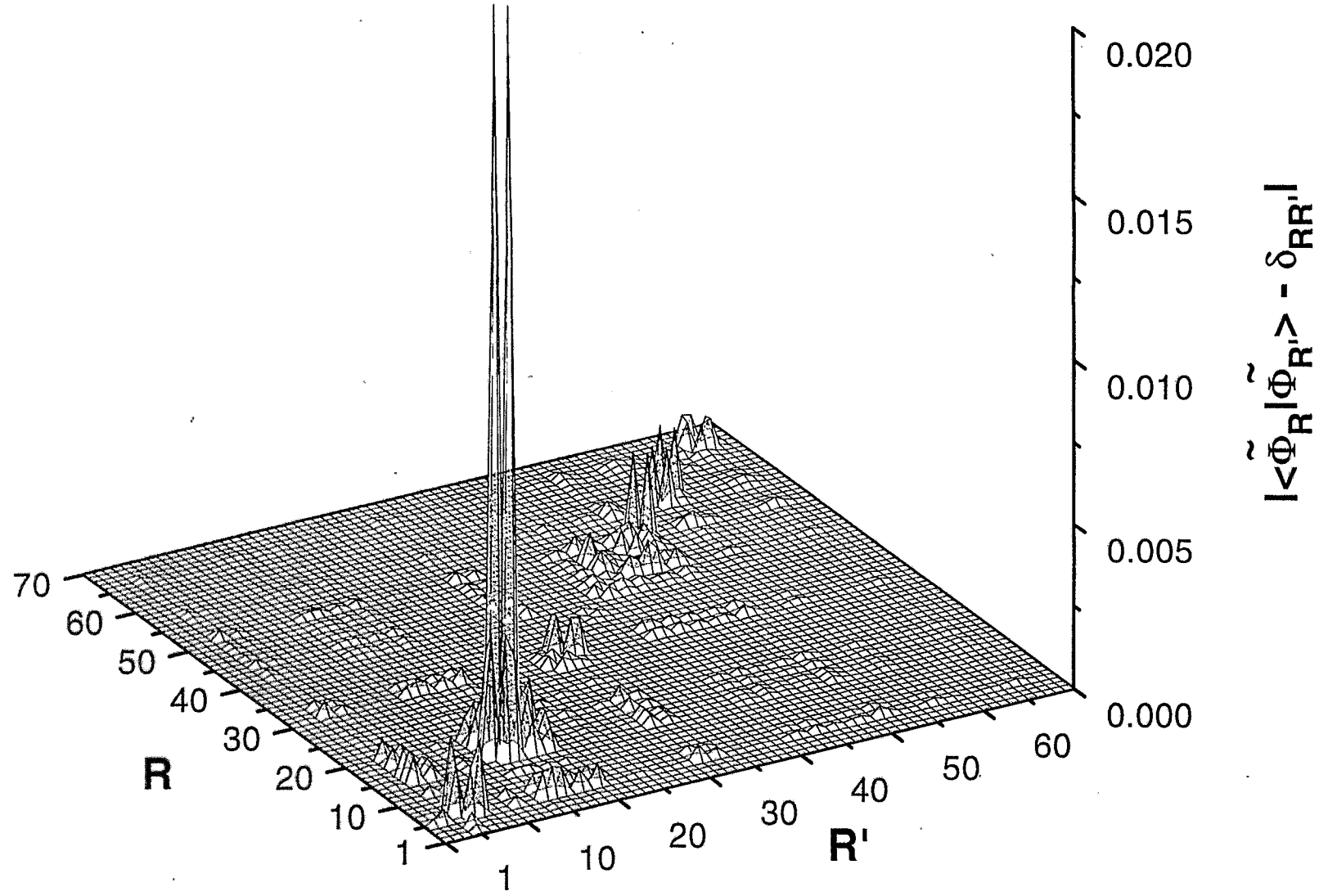

Csm, 190st, 1channel.

Fig. 1b

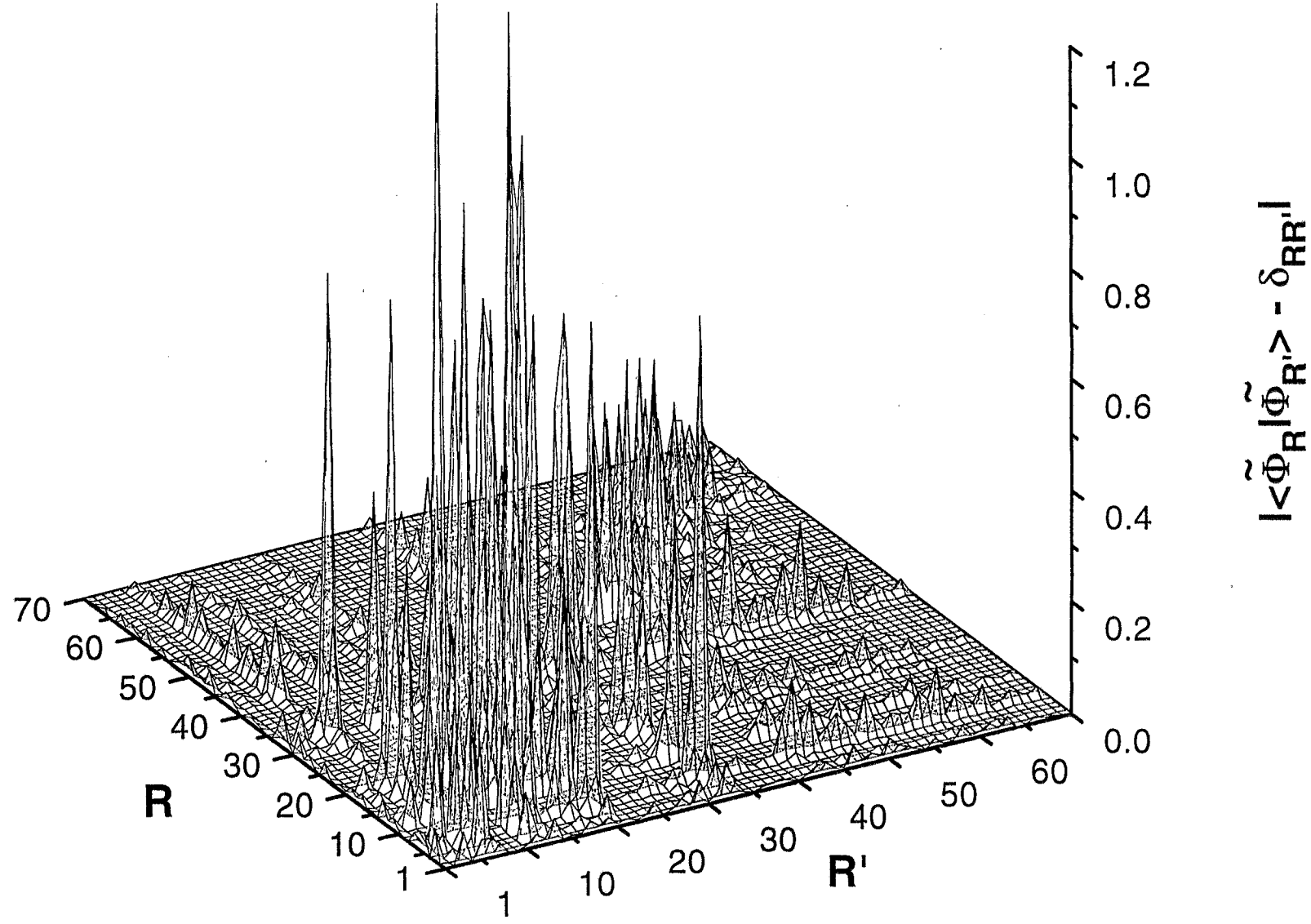

Csm, 190st, 1channel.

Fig. 1c

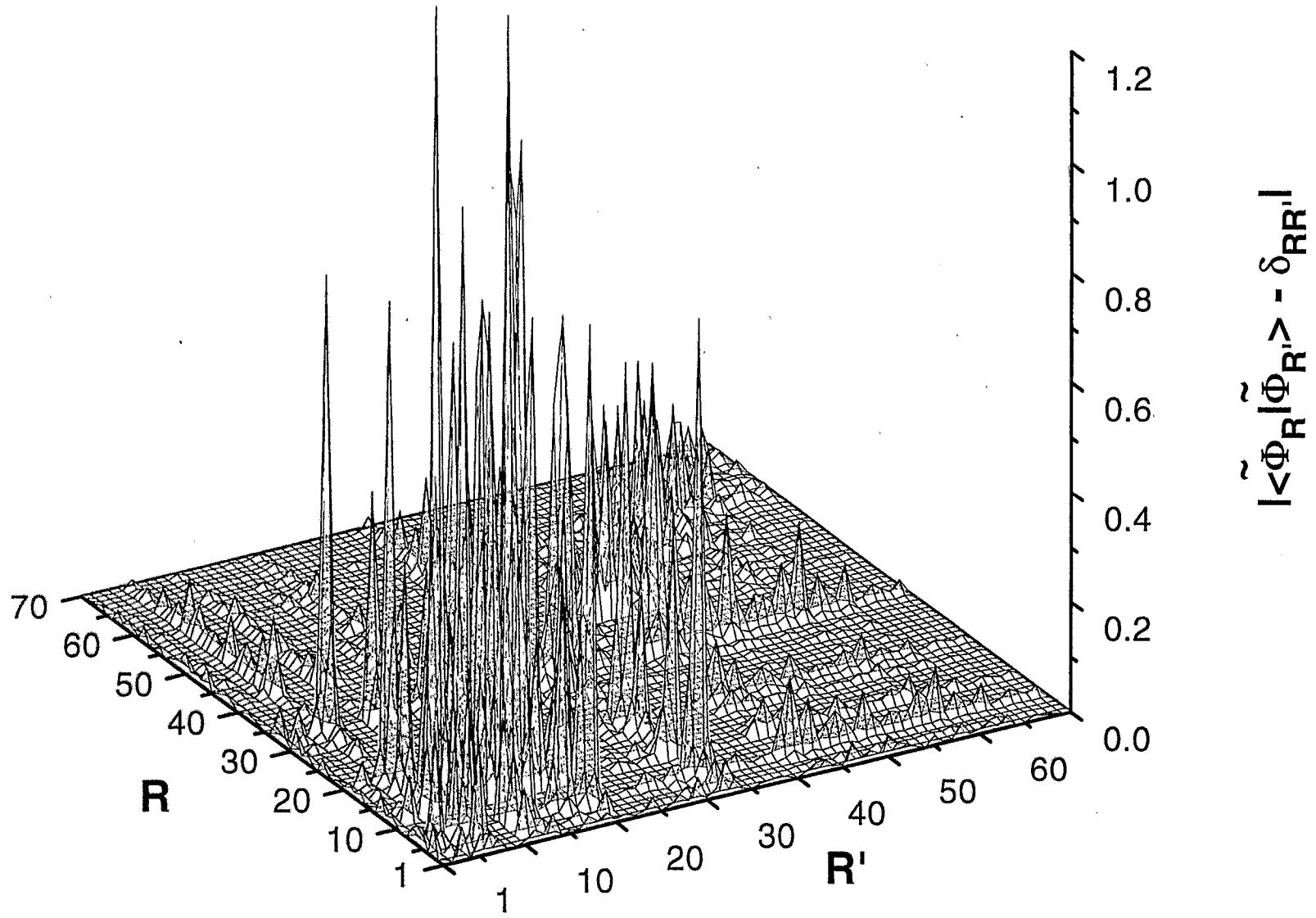

Stm, 70st, 1channel.

Fig. 1d

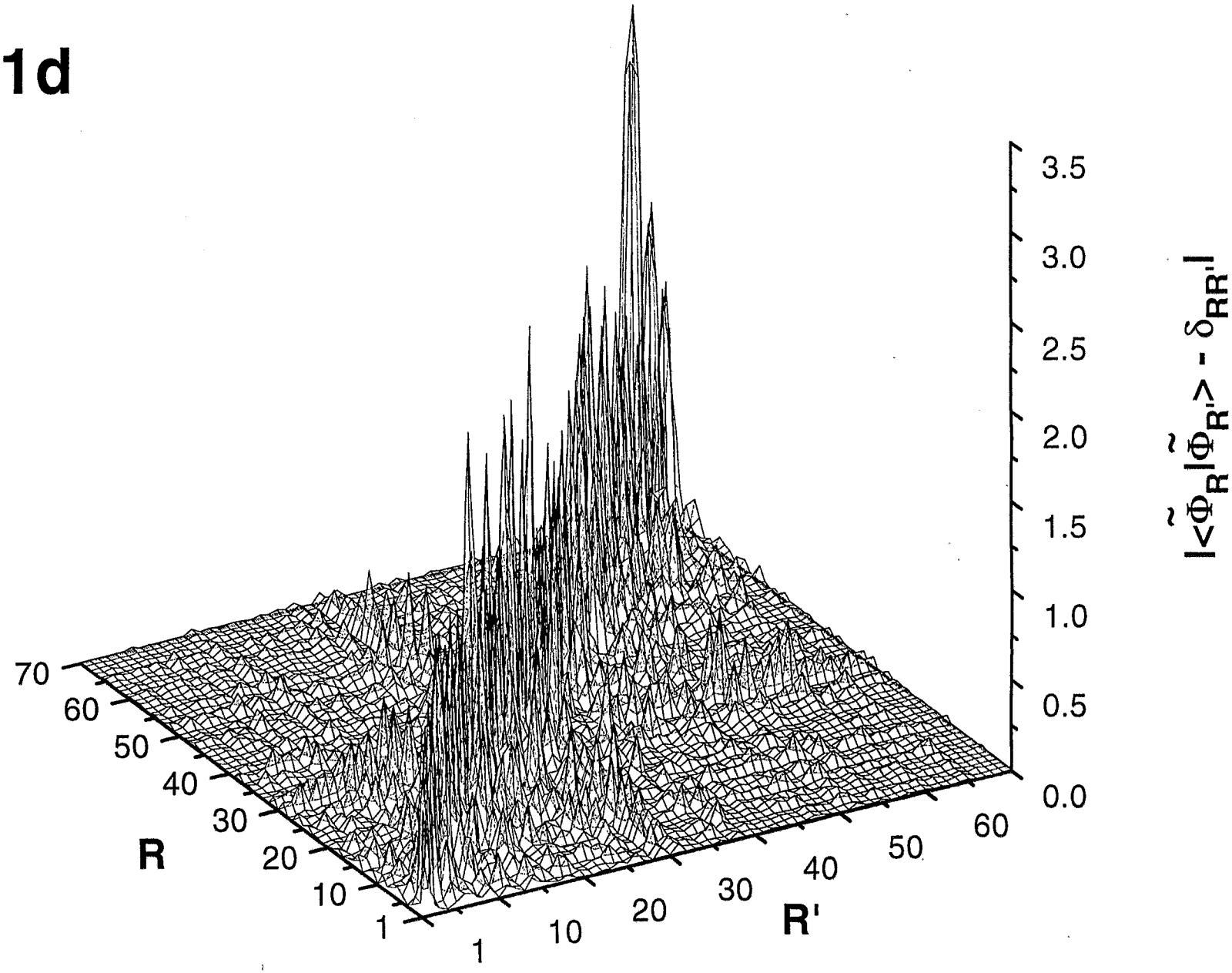

Fig. 2

Two nonsymmetrical states

Points for k_{eff} are marked

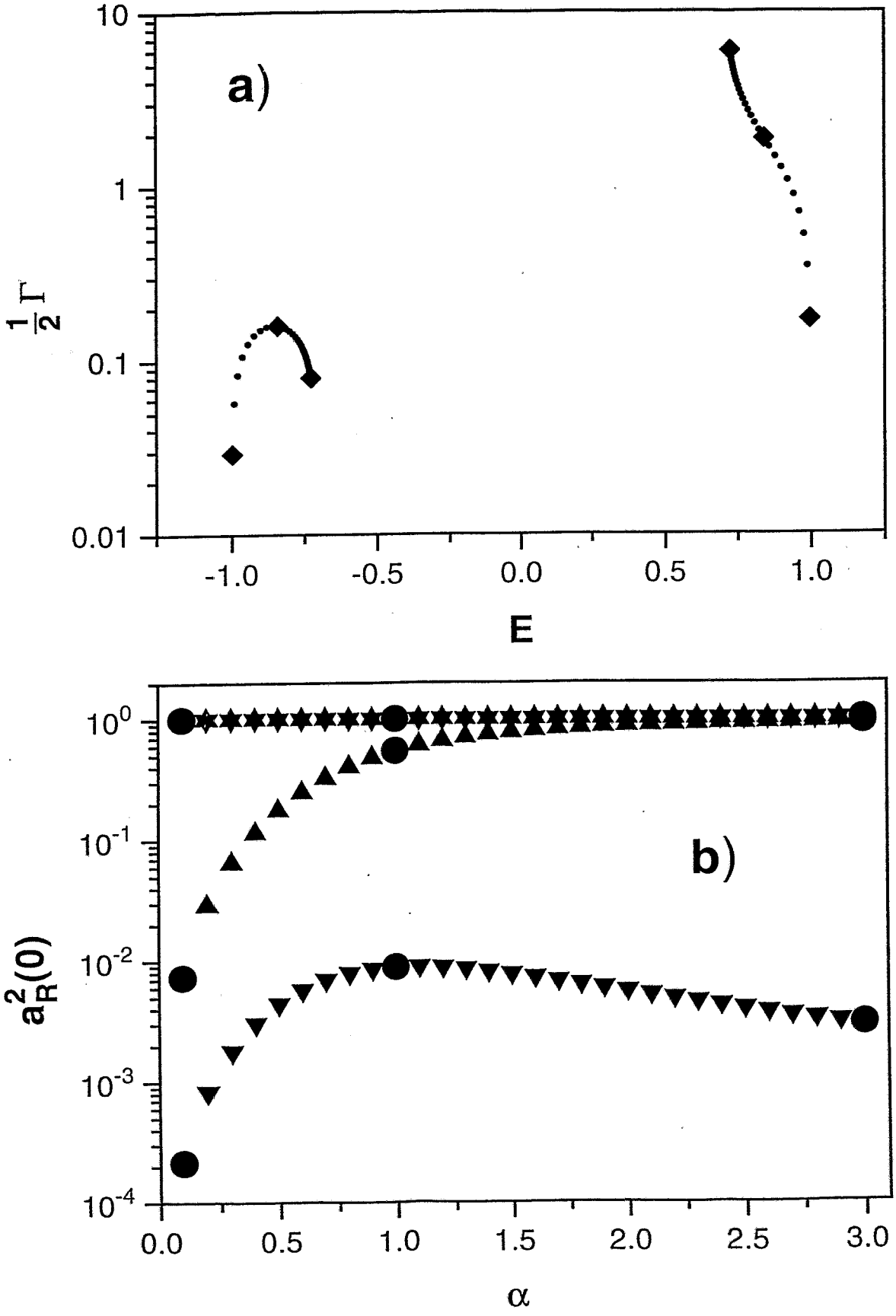

Two states. Trapped state excited.

Fig. 3

Delta shaped beam.

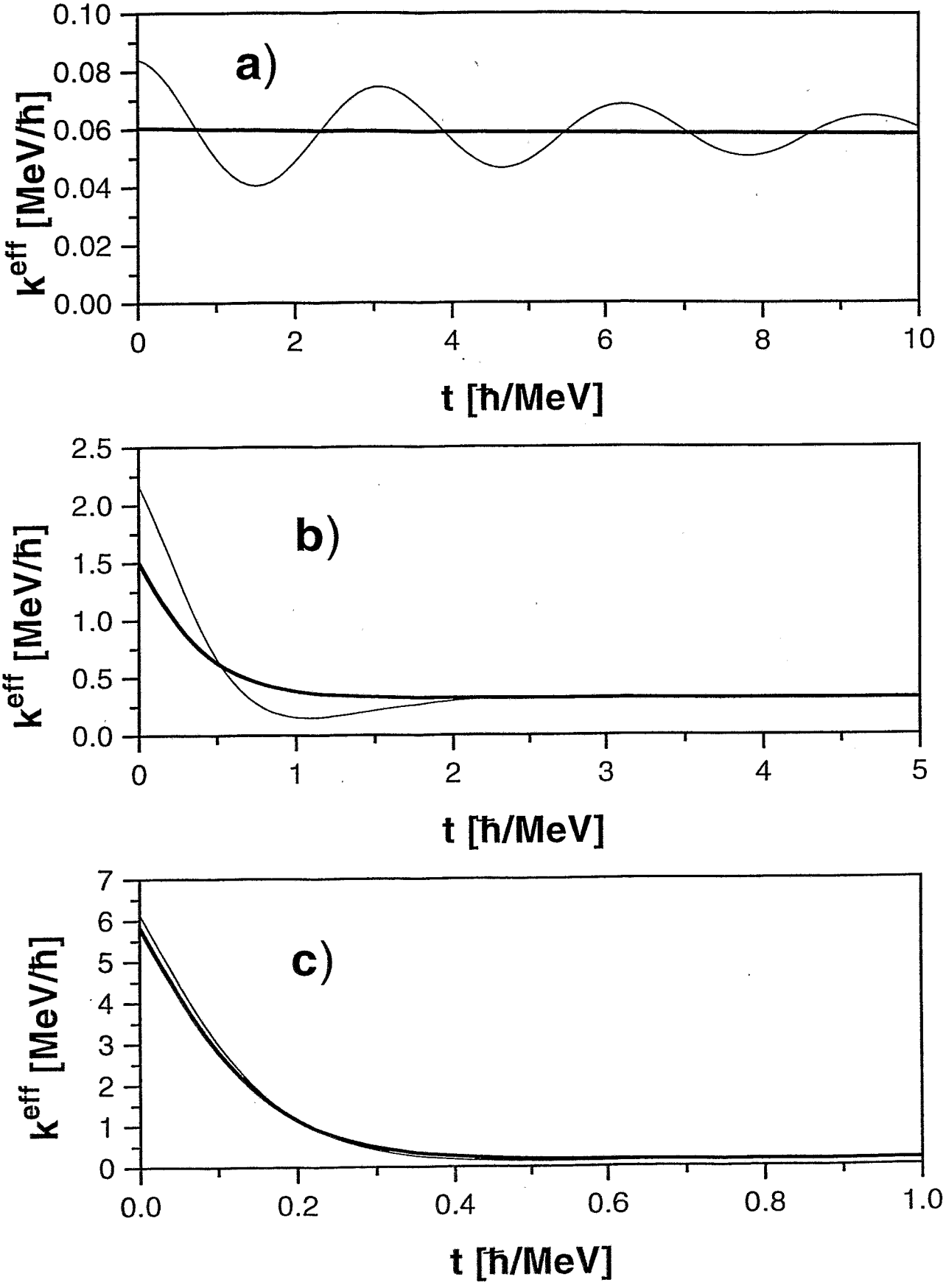

Fig. 4

Two states. Broad state excited.

Delta shaped beam.

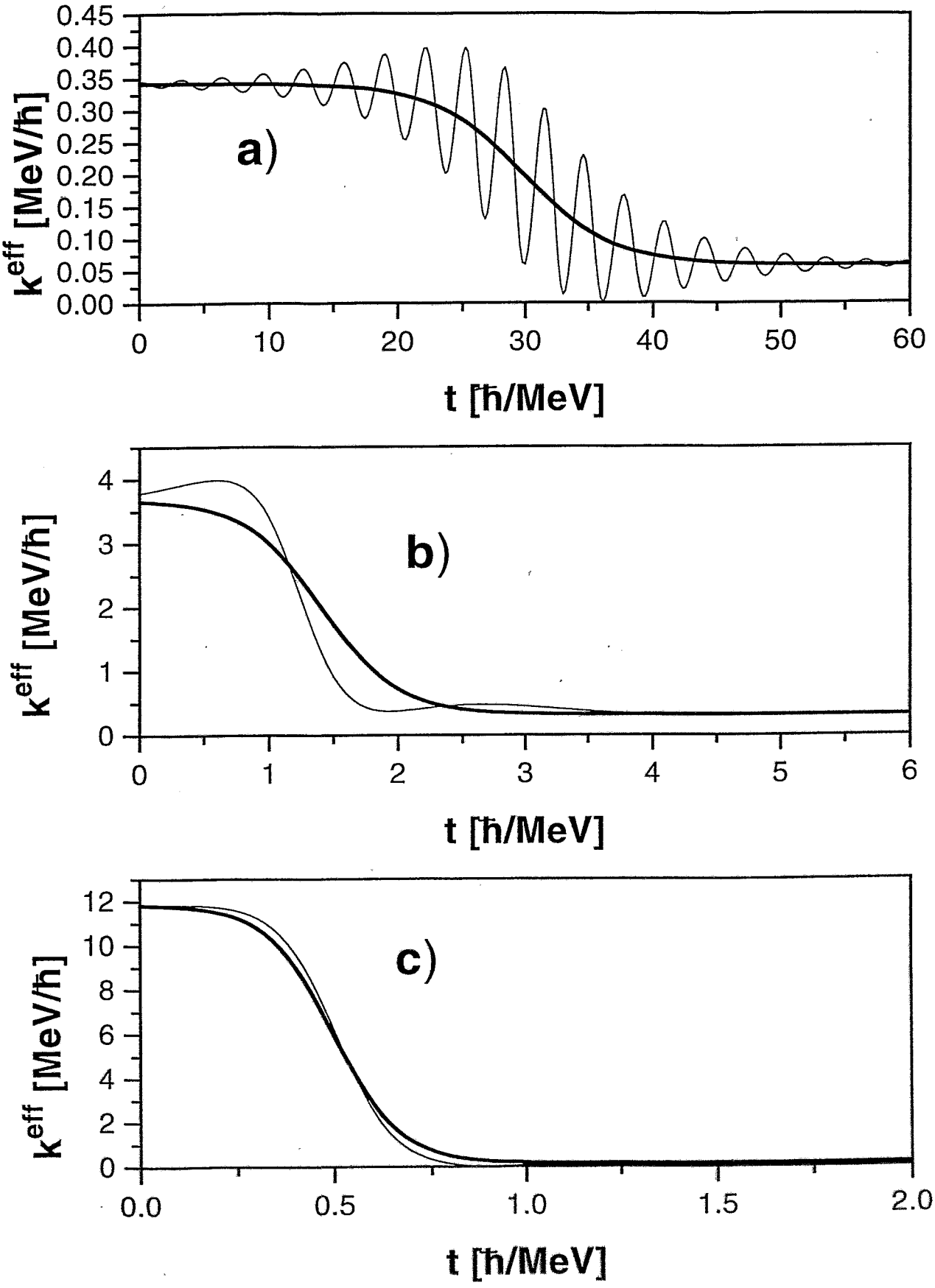

Fig. 5 **Statistical model, 70 states, 2 channels. Narrow beam, κ=10.**

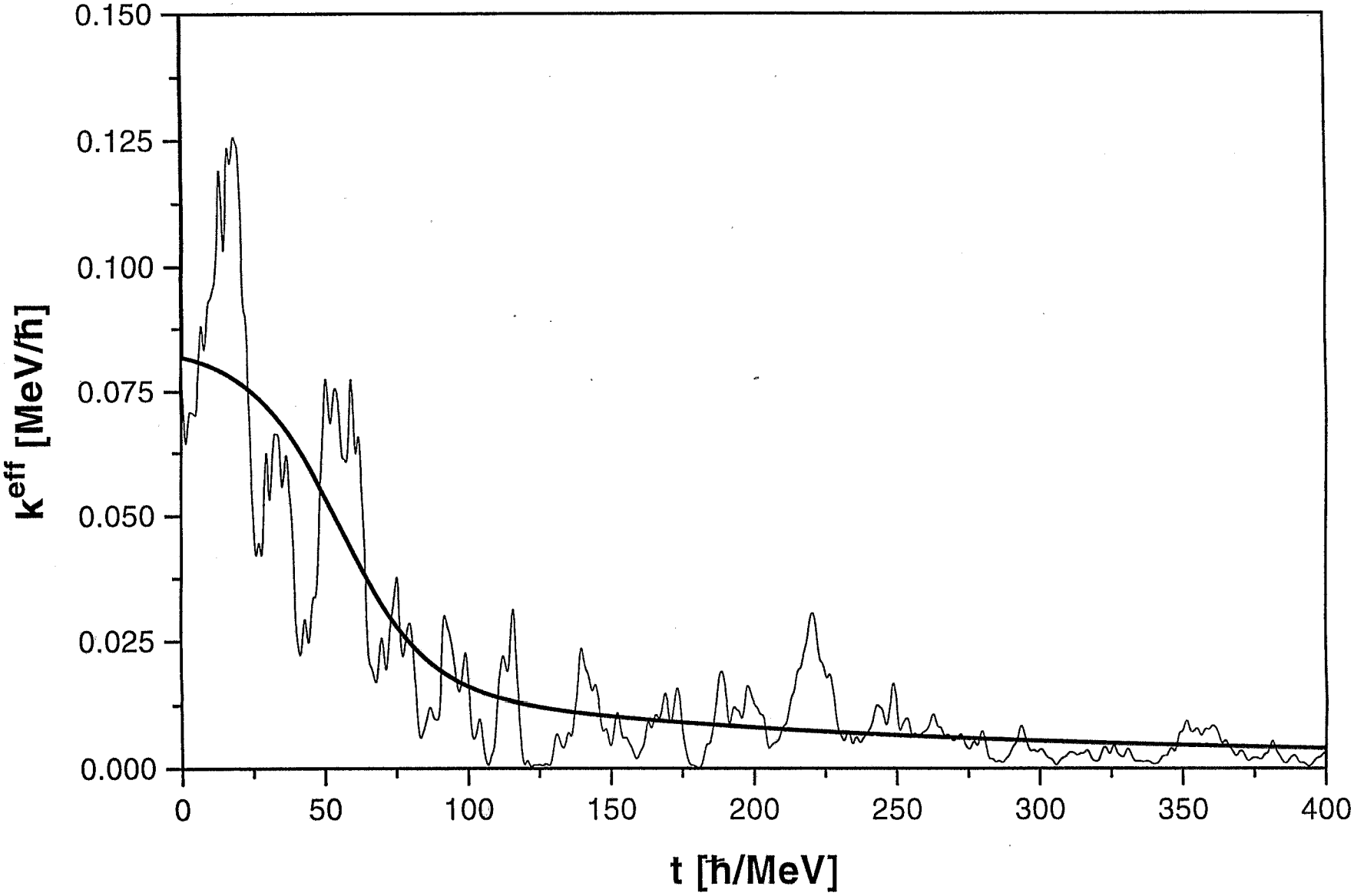

Fig. 6

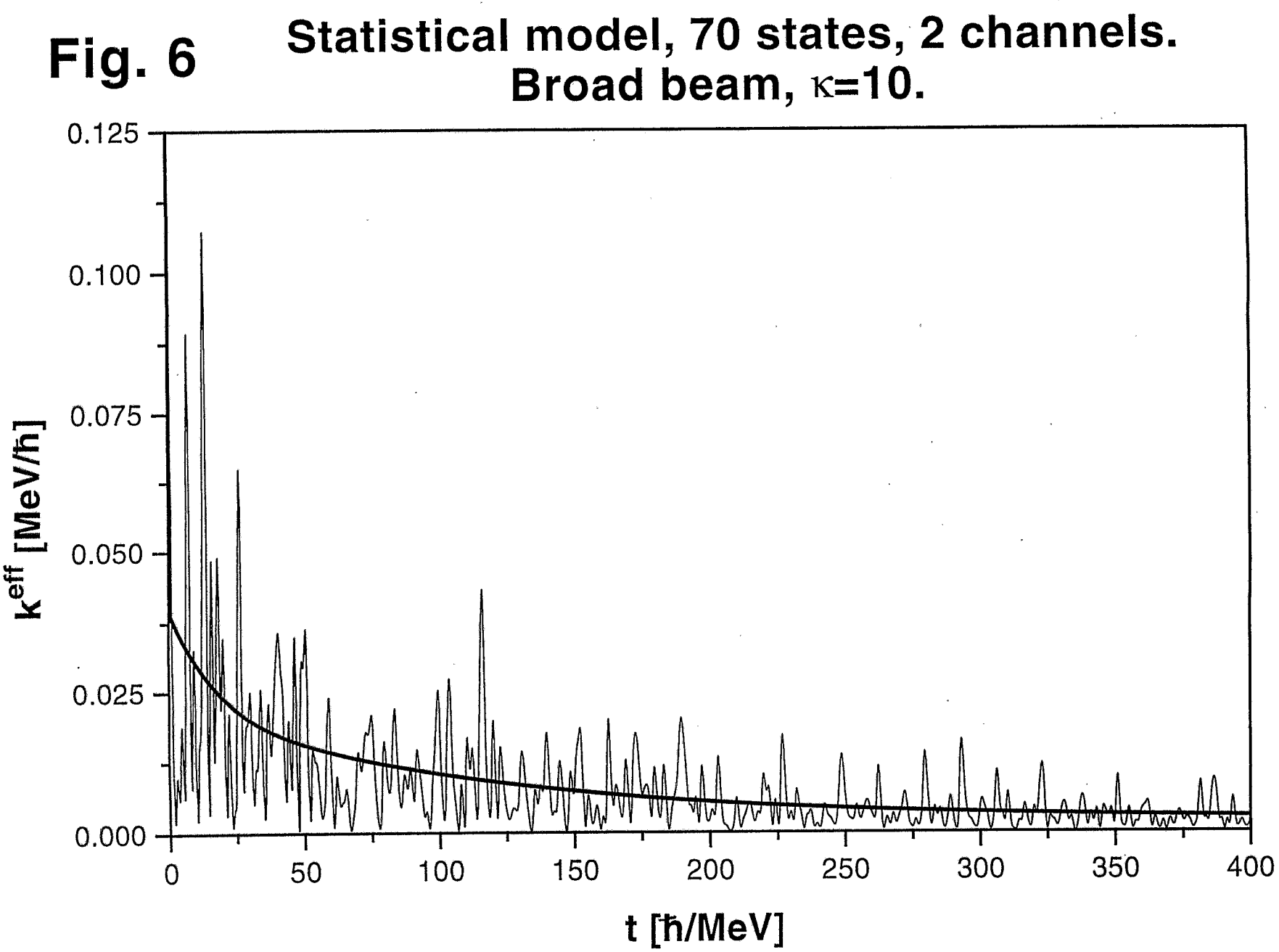
Statistical model, 70 states, 2 channels.
Broad beam, κ=10.
0.125
0.100
0.075
0.050
0.025
0.000
k^eff [MeV/ħ]
0
50
100
150
200
250
300
350
400
t [ħ/MeV]

Fig. 7 Csm, 190st, 1ch, broad beam.

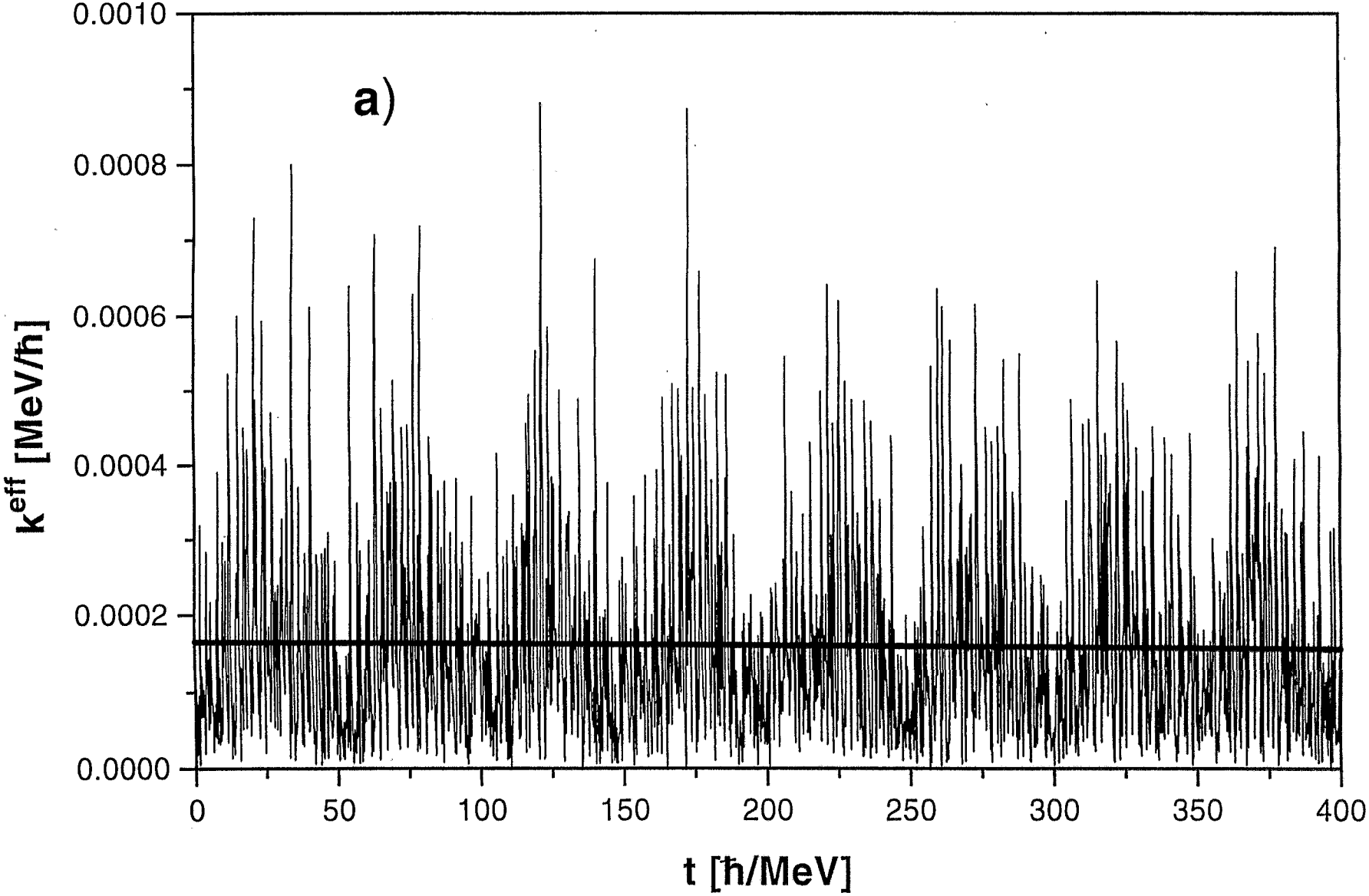

Fig. 7 **Csm, 190st, 1ch, broad beam.**

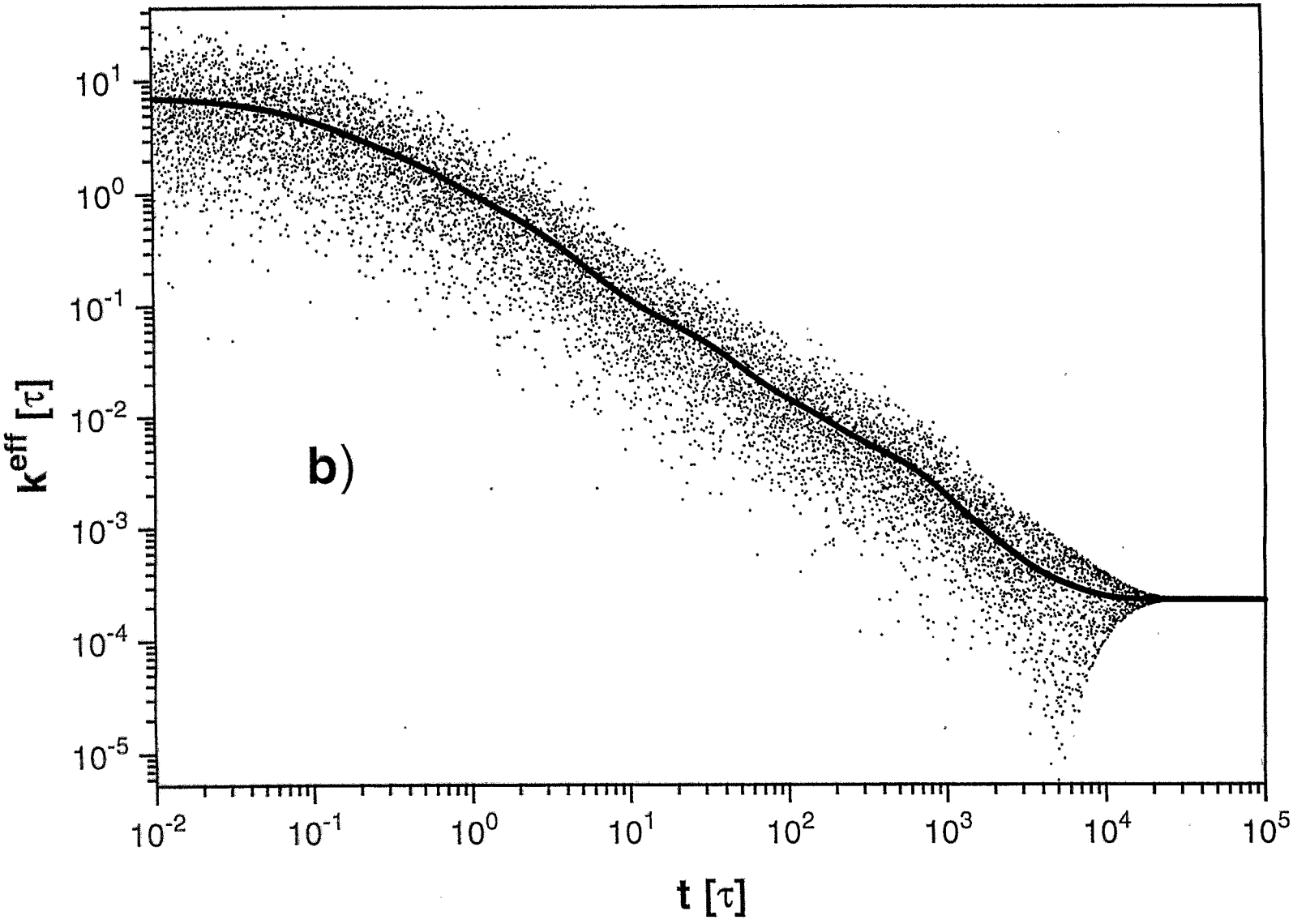

Fig. 8

Statistical model, 130 states, κ =1

Nine randomly chosen matrices.

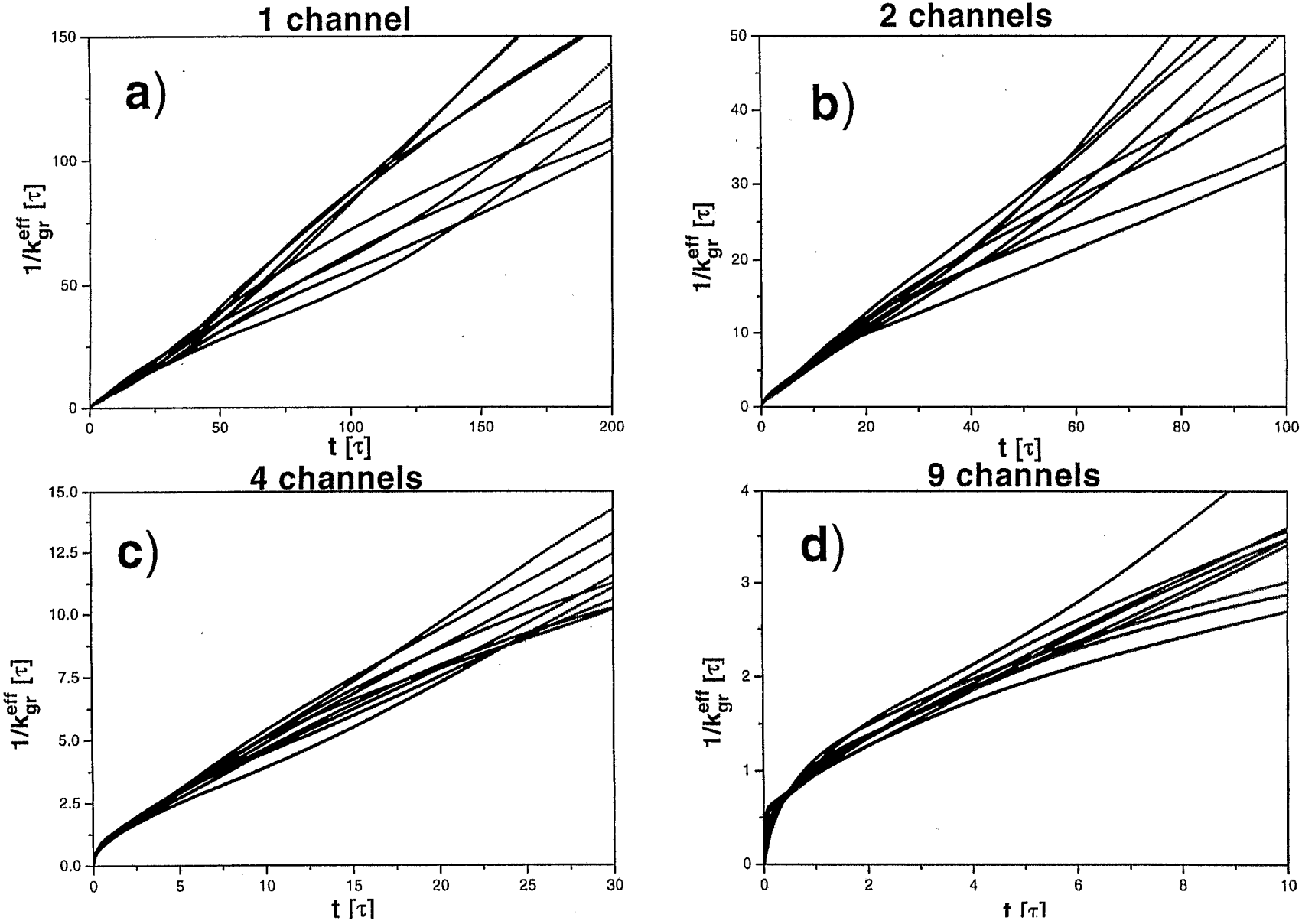

Fig. 9

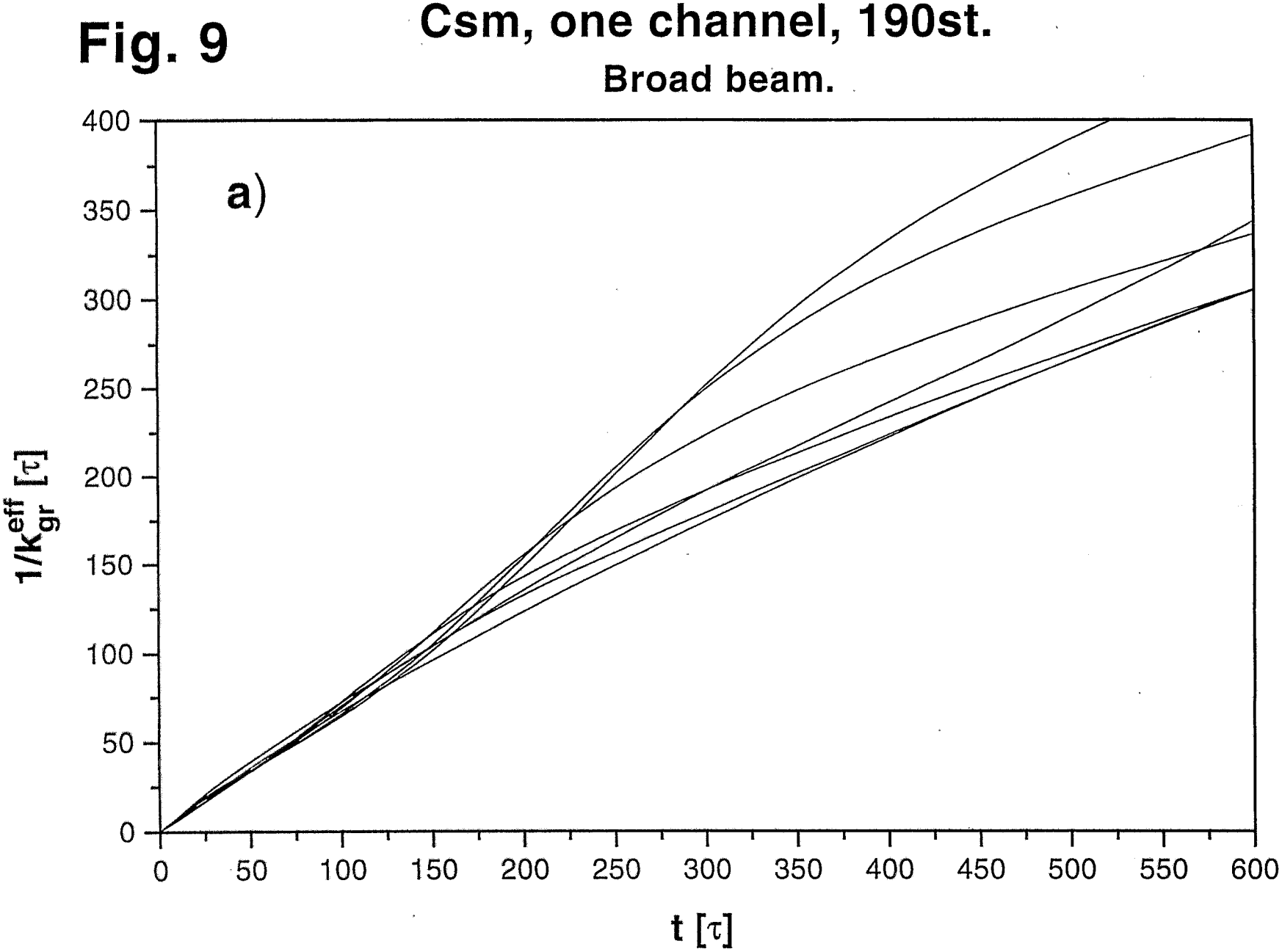
Csm, one channel, 190st.
Broad beam.
a)
400
350
300
250
200
150
100
50
0
$1/k_{gr}^{eff}$ [τ]
0
50
100
150
200
250
300
350
400
450
500
550
600
t [τ]

Fig. 9

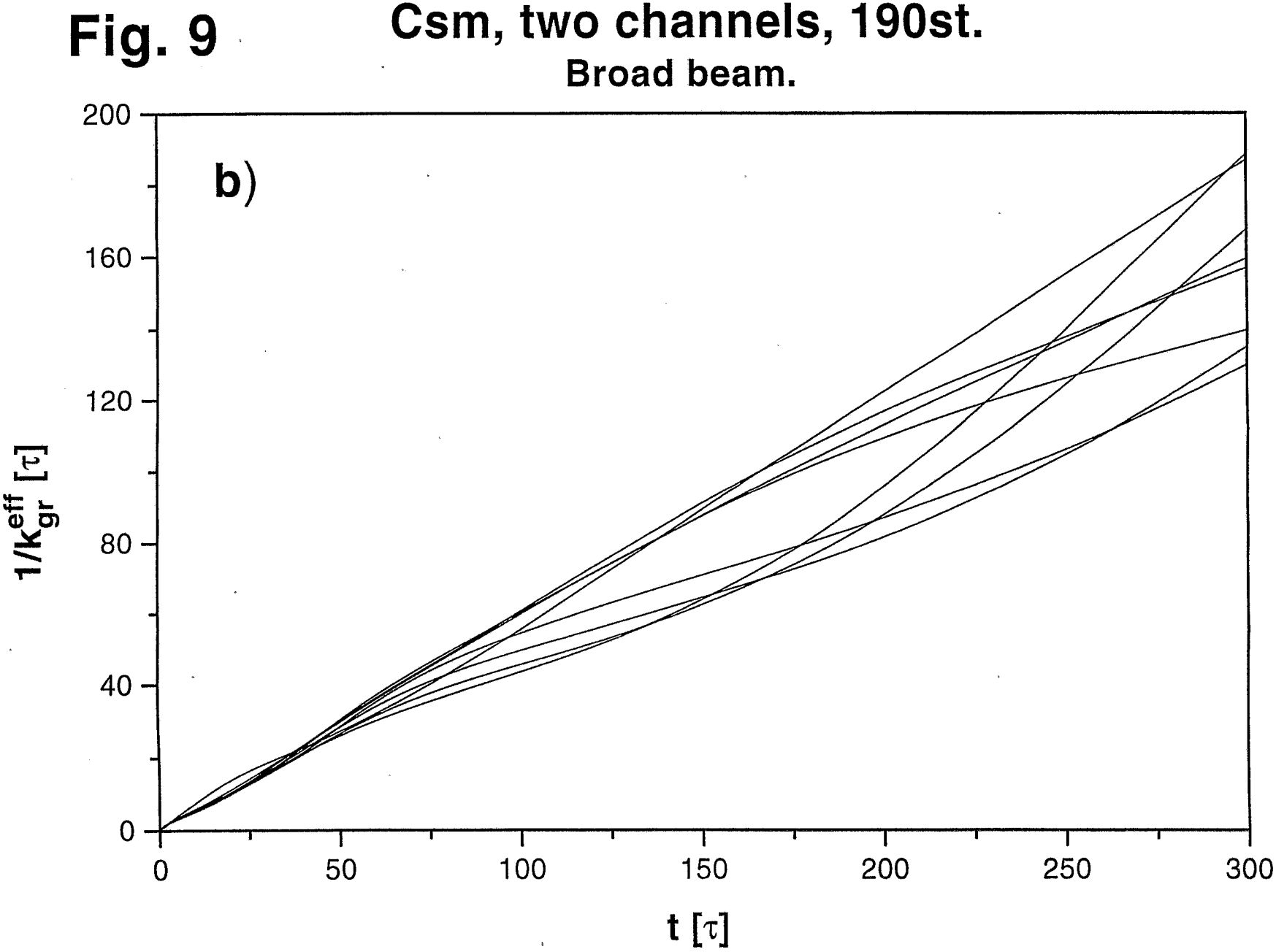
Csm, two channels, 190st.
Broad beam.
b)
200
160
120
80
40
0
0
50
100
150
200
250
300
$1/k_{gr}^{eff}$ [τ]
t [τ]

Fig. 9

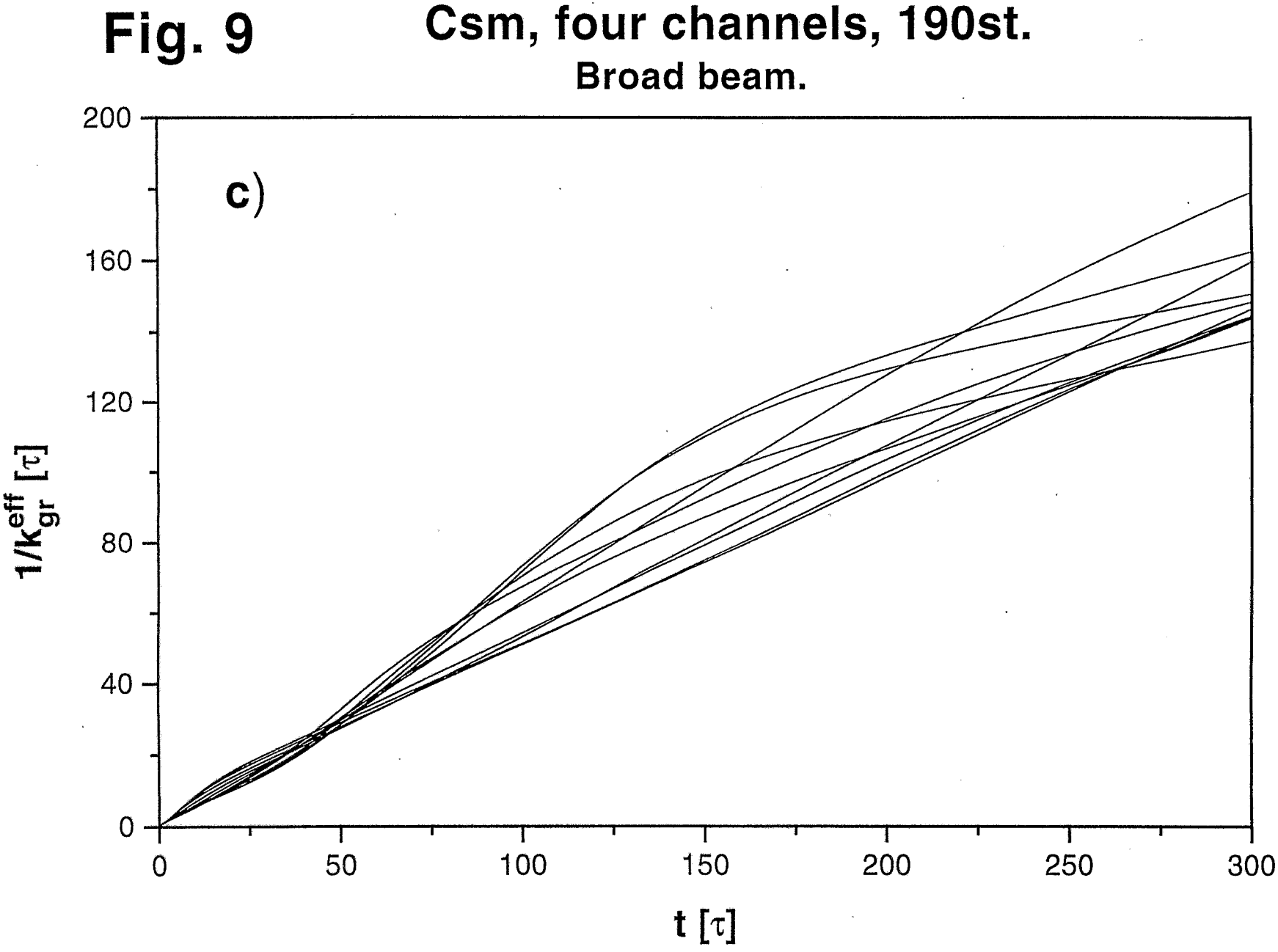
Csm, four channels, 190st.
Broad beam.
c)
200
160
120
80
40
0
0
50
100
150
200
250
300
$1/k_{gr}^{eff}$ [τ]
t [τ]

Fig. 10

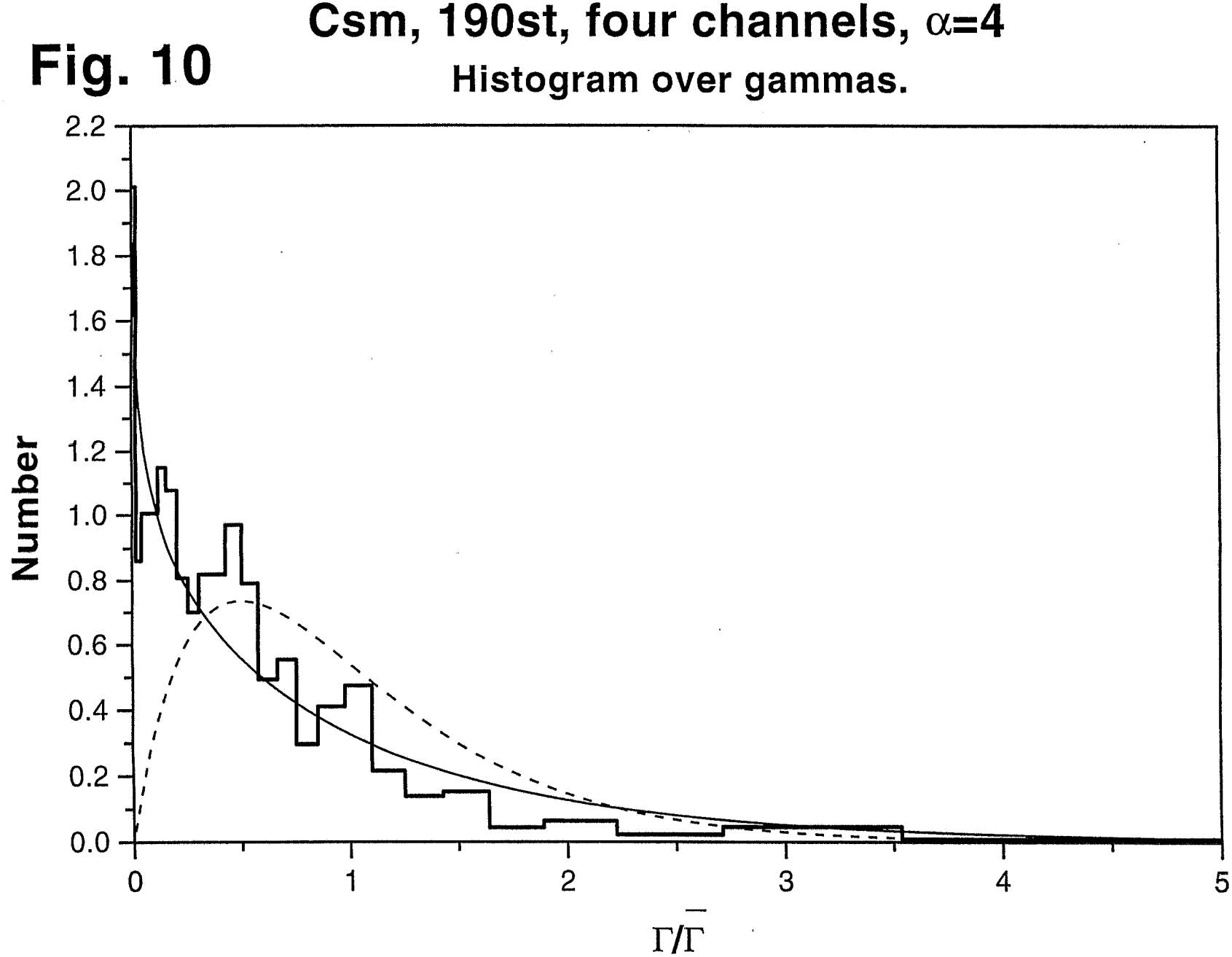
Csm, 190st, four channels, α=4
Histogram over gammas.
Number
2.2
2.0
1.8
1.6
1.4
1.2
1.0
0.8
0.6
0.4
0.2
0.0
0
1
2
3
4
5
Γ/Γ̄